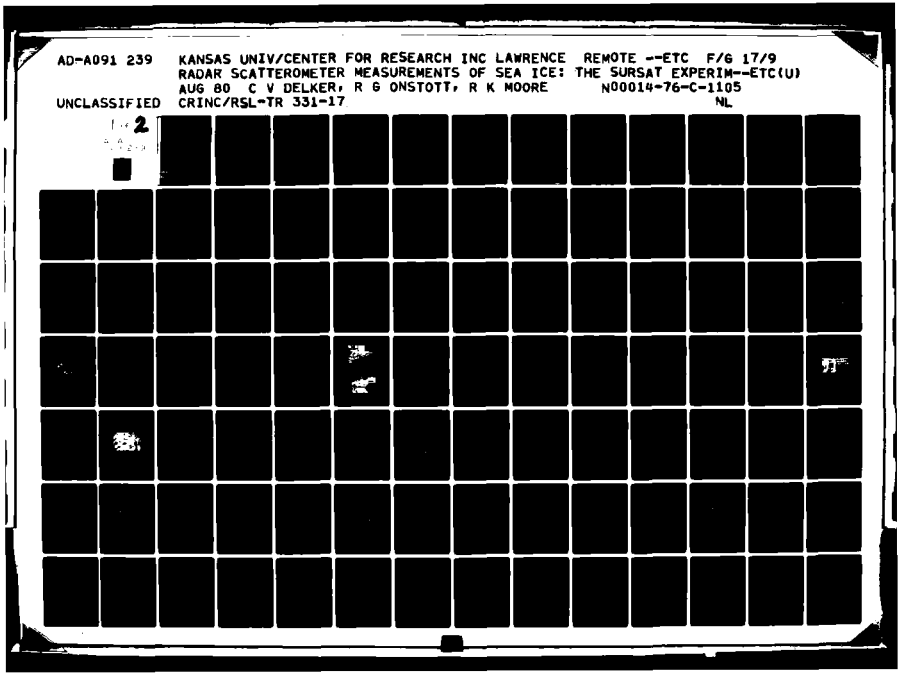
AD-A091 239
KANSAS UNIV/CENTER FOR RESEARCH INC LAWRENCE REMOTE --ETC F/G 17/9
RADAR SCATTEROMETER MEASUREMENTS OF SEA ICE: THE SURSAT EXPERIM--ETC(U)
AUG 80 C V DELKER, R G ONSTOTT, R K MOORE N00014-76-C-1105
UNCLASSIFIED CRINC/RSL-TR 331-17 NL
2

CRINC

LEVEL II

REMOTE SENSING LABORATORY

12

RADAR SCATTEROMETER MEASUREMENTS OF SEA ICE: THE SURSAT EXPERIMENT

C. V. Delker

R. G. Onstott

R. K. Moore, Principal Investigator

Remote Sensing Laboratory
Center for Research, Inc.
The University of Kansas
Lawrence, Kansas 66045

RSL Technical Report
RSL TR 331-17

August 1980

Supported by:

OFFICE OF NAVAL RESEARCH
Department of the Navy
800 N. Quincy Street
Arlington, Virginia 22217

CONTRACT N00014-76-C-1105

THE UNIVERSITY OF KANSAS CENTER FOR RESEARCH, INC.
2291 Irving Hill Drive—Campus West Lawrence, Kansas 66045

(6)

RADAR SCATTEROMETER MEASUREMENTS OF SEA ICE: THE SURSAT EXPERIMENT.

(10)

C.V. Delker
R.G. Onstott
R.K. Moore Principal Investigator

Remote Sensing Laboratory
Center for Research, Inc.
The University of Kansas
Lawrence, Kansas 66045

(14) RSL Technical Report
CRINC/RSL-TR 331-17

(11) August 1980

(12) Supported by:

OFFICE OF NAVAL RESEARCH
Department of the Navy
800 N. Quincy Street
Arlington, Virginia 22217

(15) CONTRACT N00014-76-C-1105
NR 307-383
Code 460

406618

ABSTRACT

The radar backscatter properties of sea ice were investigated by a team from the University of Kansas Remote Sensing Laboratory during the month of March 1979. These measurements were made using both a surface-based and a helicopter-borne scatterometer system. Thick first-year sea ice, thin first-year sea ice, brackish sea ice, and fresh-water inland lake ice were investigated. These ice sites were located off or near the Canadian coast at Tuktoyaktuk, N.W.T., Canada. The investigations were part of the Beaufort Sea Ice Experiment segment of the Surveillance Satellite Project (SURSAT) of the government of Canada. This paper describes the field experiment, documents the sensors used, and presents the results obtained.

Measurements in the 8-18 GHz region verify the ability of radar to distinguish between the different ice types. For angles of incidence greater than 40°, VV polarization and 9 GHz frequency appear to provide the best discrimination capability. A strong correlation between radar scattering cross-section and the salinity of ice was observed. Higher salinity ice types produced higher scattering coefficients. Effects of snow cover on lake ice was also investigated. Removal of the snow cover produced significantly lower scattering coefficients which demonstrates the importance of snow cover as a parameter in the radar backscatter return mechanisms of ice.

TABLE OF CONTENTS

LIST OF TABLES

LIST OF FIGURES

LIST OF FIGURES (continued)

LIST OF FIGURES (continued)

1.0 INTRODUCTION

Since the early part of the 1950's extensive studies of the region north of the Arctic Circle have provided a wealth of information about the area. Even so, the surface has only just been scratched and many more investigations are needed. In recent years the discovery of large mineral deposits in this area has generated increased interest and a demand for more information about the region. The scientific, commercial, and military communities have all taken an active part in this quest for more knowledge about the Arctic Ocean and the sea ice that covers it.

The University of Kansas Remote Sensing Laboratory's Sea Ice Group is involved in the use of state-of-the-art microwave remote sensing equipment to perform studies of the radar backscatter properties of sea ice. The research performed by this group is directed toward selecting the optimum radar parameters (angle of incidence, frequency, and polarization) for use in the design of polar reconnaissance and mapping radars which will meet the requirements of commercial and military users.

1.1 The Arctic

The oceans of the world account for almost 71 percent of the earth's total surface area and during the winter season approximately 12 percent of these waters may be covered by sea ice. As its name implies, sea ice is frozen sea (salt) water. The Arctic Ocean is partially covered by sea ice at all times.

Sea ice is a dynamic substance. Unlike the land masses which cover the remainder of the earth's surface and which are normally

very stable, sea ice is in continuous motion due to the currents of the ocean and the wind. The physical characteristics and area of coverage of the ice also change rapidly as temperature varies. These dynamic characteristics of sea ice make surface operations and navigation in this region very hazardous. The desire for at least daily information in the form of large-area maps and forecasts of movements of the ice cover is shared by everyone involved in Arctic operations.

The Arctic region can be divided into two areas called the maritime Arctic and the maritime sub-Arctic [1]. The maritime Arctic is defined by the average extent of the perennial (multi-year) ice cover. The nations which border the maritime Arctic are the Soviet Union (44 percent), Canada (23 percent), Denmark-Greenland (14 percent), Norway (11 percent), and the United States (8 percent). The maritime sub-Arctic is defined by the average extent of the annual or one-year ice cover. Nations which have borders included in the maritime sub-Arctic are mainland China, East and West Germany, Finland, Iceland, Japan, Poland, and Sweden. As this list of countries indicates, many nations have a direct interest in the study of sea ice.

Arctic sea ice consists of a wide variety of types which are characterized by age, thickness, and the process of formation. A list of categories utilized by Parashar et al. [2] differentiates between seven ice types:

1) Open water
2) New ice 0-5 cm
3) Thin young ice 5-18 cm
4) Thick young ice 18-30 cm
5) Thin first-year sea ice 30-90 cm
6) Thick first-year sea ice 90-180 cm
7) Multiyear sea ice 180-360 cm.

With the onset of winter, sea ice begins to form first in the shallow waters near the coastal regions. As the winter season progresses this ice sheet spreads out to meet the pack ice and the entire surface of the Arctic Ocean becomes covered with ice. By spring, the ice in the coastal regions is mostly thick first-year sea ice which is characterized by a flat smooth surface. Floes of thick first-year sea ice have edges which are angular as contrasted with multiyear sea ice floes which have rounded edges. Multiyear sea ice, which makes up the majority of the pack ice, is characterized by a rolling surface created during the summer melt season. Melting conditions alter the material properties of the ice as well as the surface features, creating a distinct difference between multiyear ice and the newer ice.

The pressure ridge is another feature of sea ice that is very important to people operating in the Arctic. A pressure ridge is formed by the collision of two ice floes. The collision causes the edges of the floes to buckle and fracture into large blocks of ice which are deposited on the surface to form what is referred to as the sail of the pressure ridge. Blocks of ice are also forced beneath the surface of the floes and form the keel of the pressure ridge. The ratio of sail height to keel depth may be as much as 1:10. Consequently, even a small-sail ridge can present a big obstacle to surface vessels operating in the region.

With the discovery of large mineral deposits, particularly offshore petroleum, operations in this region are expanding rapidly. Companies interested in exploiting these minerals are very concerned about the ice cover and its movements. These companies desire to

conduct their operations on a year-round basis; but the ice can cut off shipping which is necessary to service and supply the operations, hinder the movement of tankers which are removing gas and oil and threaten offshore drilling rigs.

Military movements of submarines, surface vessels, and troops in the Arctic region also require detailed information about the ice cover. Recent policy decisions advocating energy independence for the United States make the oil fields located off the north slope of Alaska strategically important and increase the role of the military in the region.

The ice cover of the Arctic Ocean also plays an important part in the global weather picture. During one revolution of the earth, the polar regions lose more heat to space than is received from the sun. Heat from the lower latitudes is circulated into the polar regions to compensate for this heat loss. The polar regions are the heat sinks in the global thermodynamics cycle of atmosphere and ocean. For this reason, meteorologists desire information about the ice cover for use in long-range weather forecasting and for supplying short-range weather information to the people living and operating in the Arctic.

All of these endeavors require knowledge about the ice cover on a continuing basis. Major parameters of interest are the thickness of the ice, the area of coverage of the ice, and the strength of the ice. The scientific community, in trying to meet these needs, has conducted a number of experiments in the past few years in the Arctic.

1.2 Remote Sensing of Sea Ice

Presently the greatest need of Arctic operations is to obtain maps of large areas of the Arctic on a daily basis so that the movements of the ice can be monitored and forecast. This is necessary to make navigation as safe as possible and to find the most economical and quickest routes through the ice. Conventional aerial photographic methods using black-and-white, color, and infrared films and visual observations from aircraft have been used in the past to map large areas of sea ice. These methods of mapping are at the mercy of weather and lighting conditions. The expense of covering large areas is also a disadvantage for this type of mapping.

The development of microwave remote-sensing imaging radars provides an alternative to photographic techniques. Radar images are comparable to those produced by photographic techniques; but, since a radar imager provides its own illumination, it can operate equally well in day or night conditions, and in most instances the radar imager is virtually independent of weather conditions. These features make radar imagers especially well-suited for mapping in the Arctic regions.

Studies of the applicability of side-looking airborne radar (SLAR) systems for research and reconnaissance of sea ice began as early as 1962 when the U.S. Army Cold Regions Research and Engineering Laboratory conducted experiments using a U.S. Air Force AN/APQ-56 K-band SLAR [3]. These experiments verified the feasibility of using SLAR systems to obtain good-resolution images of sea ice and proved the ability to map large expanses of sea ice independent of incident light and weather conditions.

Studies of sea ice using radar systems operating in the 1-18 GHz frequency range have proliferated since that time. Experiments by Rouse [4], Johnson and Farmer [5], Glushkov and Komarov [6], Ketchum and Tooma [7], Parashar et al. [2], Dunbar [8], Dunbar and Weeks [9], Gray et al. [10], Ketchum [11], Onstott et al. [12, 13], and Patel et al. [14] have demonstrated the ability of radar systems to discriminate between different ice types and to evaluate sea ice conditions.

Earlier studies of sea ice using radar systems, particularly SLAR experiments, made use of radar systems which were readily available but which had been designed for purposes other than mapping sea ice. This has resulted in a great deal of qualitative information about the interaction of microwaves with sea ice but very little quantitative information which could be used for the design of radar systems optimized for sea ice mapping.

Recognizing the need for more detailed information about the interaction of microwaves with sea ice, the Sea Ice Group of the University of Kansas Remote Sensing Laboratory embarked on a series of measurement programs using a scatterometer system with multi-angle, multi-frequency, and multi-polarization capabilities designed to fill this void. Scatterometer measurements had been made prior to this time but the sensors were usually airborne, so that collecting surface-truth information about the extensive areas covered was difficult. The University of Kansas experimental procedure was designed so that surface-truth measurements of the snow and ice conditions in the area of the radar footprint could be made at the time of the backscatter measurements. This surface-truth information is necessary for the

determination of relationships between radar backscatter and the target properties.

1.3 University of Kansas Sea Ice Experiments

The University of Kansas Sea Ice Group has conducted three experiments in the Arctic. These experiments occurred during May 1977, April 1978, and March 1979. Data were collected using a transportable surface-based scatterometer system (TRAMAS) and a helicopter-borne scatterometer system (HELOSCAT). The HELOSCAT system was first implemented in 1978 and greatly enhanced mobility and the ability to investigate remote ice sites.

Ice types investigated during these experiments included fresh-water inland lake ice, thick first-year sea ice, thin first-year sea ice, brackish sea ice, multiyear sea ice, and a pressure ridge. These experiments are summarized in the following sections.

1.3.1 May 1977 Experiment

The first sea ice backscatter experiment in this series was conducted during the month of May 1977, at Point Barrow, Alaska. The Naval Arctic Research Laboratories (NARL) served as a base of operations. The TRAMAS system was used and was transported from site to site using a snowmobile and sled. Thick first-year sea ice, multi-year sea ice, a pressure ridge, and two fresh-water lakes, one of which was frozen to the bottom, were investigated. Results of the experiment indicated that there were combinations of the radar parameters which provided a good ability to discriminate among the ice types studied. For most of the frequencies used the radar cross-section σ^0 showed that multiyear sea ice gave the highest return while

lake ice gave the lowest return. The radar cross-sections of the pressure ridge and thick first-year sea ice fell in between.

1.3.2 April 1978 Experiment

The April 1978 sea ice experiment also took place at Point Barrow, Alaska and was also based at NARL. The TRAMAS and the HELOSCAT systems were both utilized for this experiment. Investigations with the TRAMAS system were limited to thick first-year sea ice close to the shore due to the extremely rough ice surface conditions existing at that time. Investigations of thick first-year and multiyear sea ice were accomplished with the HELOSCAT system.

The results of the HELOSCAT experiment were somewhat disappointing. Equipment malfunctions resulted in only the data collected for the 60° incidence angle being accurate. These returns correlated well with the TRAMAS data, which indicated a promising future for the HELOSCAT system once the equipment problems were corrected.

Analysis of the TRAMAS data for both 1977 and 1978 allowed conclusions about the best combination of radar parameters to be drawn. It was determined that 9 GHz, VV (vertical transmit, vertical receive) polarization, and an angle of incidence (from vertical) greater than 25° provided the greatest discrimination of the ice types studied. While the angle of incidence chosen may not allow different ice types to be differentiated by radar return alone, image interpretation greatly enhances the ability to distinguish ice types. For instance, pressure ridges can be identified as narrow linear features, which are often very bright in imagery. Thick first-year ice floes may be distinguished from multiyear ice floes by shape. Thick first-year sea

ice floes are smooth-surfaced with angular edge features. Multiyear sea ice floes have a rough rolling surface with rounded edge features. Chances of proper identification of ice types is increased by study of the imagery for tonal quality, shape, and features which aid in the discrimination of ice types.

1.3.3 March 1979 Experiment

The March 1979 experiment was a part of the Beaufort Sea Ice Experiment segment of the Canadian SURSAT (Surveillance Satellite) Project. Experiment sites were located off the Canadian coast near Tuktoyaktuk, N.W.T., Canada. Participants in the project included researchers from Canadian and United States government and university research facilities, and also personnel from several major oil companies. Research activities were supported by the Canadian Polar Continental Shelf Project (PCSP) base camp located at Tuktoyaktuk.

The TRAMAS and the HELOSCAT systems were both operated during this experiment. Thick first-year sea ice, thin first-year sea ice, brackish sea ice, and a fresh-water inland lake were investigated. The HELOSCAT system performed well during this experiment. Results compare well with those obtained with the TRAMAS system in terms of the slopes of radar cross-section versus angle of incidence and the ordering of the returns from different ice types. There is a difference in the absolute level of the HELOSCAT returns as compared with the TRAMAS returns. A problem with the calibration of one or both of the systems may be responsible for this difference.

The results of this experiment indicated a strong correlation between the salinity of the ice and the radar return. Thin first-year

sea ice, which has the highest salinity of the ice types studied, also demonstrated the highest radar cross-section (note that multiyear ice was not present -- it gives a very strong return). Lake ice, which has a very low salinity, also had the lowest radar cross-section. The lake ice site was also studied for response to snow cover. The results of this experiment were very dramatic. Lake ice with the snow cover removed to provide a bare surface had an average of 8 dB lower radar cross-section than the snow-covered surface.

The March 1979 experiment is the topic of the remainder of this paper. Chapter 2 deals with the theory and sensor documentation. Chapter 3 describes the experiment location, procedures, and surface truth. Chapter 4 is a presentation of the results and Chapter 5 contains a comparison of these results with the results of the 1977 and 1978 experiments.

1.3.4 The 1980 Experiment

The HELOSCAT system will be operated as a part of the YMER-80 expedition scheduled for August 1980. This expedition is funded by the Swedish Natural Science Research Council and the Swedish government. The icebreaker YMER will serve as a floating research station as it sails into the Arctic Ocean from Tromso, Norway. Researchers from a number of nations are scheduled to participate in a wide variety of experiments during this expedition.

2.0 RADAR THEORY AND SENSOR DESCRIPTION

This chapter presents a brief discussion of radar theory as it applies to the radar scatterometer and the measurements to be presented in later chapters. Documentation and a description of the sensor systems, TRAMAS and HELOSCAT, used in this experiment are also presented.

2.1 The Radar Scatterometer

The term radar is an acronym for radio detection and ranging. Originally the term applied to instruments developed for the purpose of detecting and measuring the range to distant objects with radio waves. Today the term radar loosely describes a broad class of devices which operate in or near the microwave region of the frequency spectrum and which have capabilities far more sophisticated than the original ranging and detection radars.

There are two general classes of microwave sensors. Passive sensors are those which measure electromagnetic radiation in the microwave range that originates from some point other than the sensor. A microwave radiometer is an example of a passive sensor. Active sensors are those which provide their own illumination. The radar imager and radar scatterometer are examples of active sensors.

A scatterometer is defined by Moore [15] as a calibrated instrument designed to measure σ^o as a function of incidence angle. σ^o is the scattering coefficient (also known as the differential scattering cross-section, or scattering cross-section per unit area), a quantity which is used to describe the scattering properties of a target independently of the radar parameters.

An imaging radar may function as a scatterometer if it is calibrated. The scattering coefficient may be determined for each point in the image, which provides the capability to study a large area and a number of diverse targets at the same time. Very few imaging radar systems are calibrated however, and even they suffer from the disadvantage of providing information at only one angle of incidence for each point observed.

Much more detailed observations may be made using a special purpose sensor called a radar scatterometer. The radar scatterometer often has multi-angle, multi-frequency, and multi-polarization capabilities. This allows detailed study of the variations of the scattering coefficient for various combinations of incident angle, frequency, and polarization. A radar scatterometer that is surface-based also has the advantage of being able to pinpoint the exact area on the surface that is being observed so that "surface truth" information, which provides a detailed description of the target, may be collected. The disadvantages of the airborne radar scatterometer relative to a SLAR include degraded resolution and a reduced area of coverage, but these are not important for surface-based operations, for which too-fine resolution may be a problem.

The purpose of the radar scatterometer is to make accurate (calibrated) measurements of the scattering coefficient for many different targets. This information can then be used to specify the optimum parameters for new radar systems, such as imaging radars, for surveillance of sea ice. The relationship of the scattering coefficient to the radar parameters is discussed in the next section which presents a derivation of the σ^{o} equation.

2.2 The Radar Equation

Just as the geometry of right triangles has the Pythagorean Equation, thermodynamics has the First and Second Laws, and electromagnetics has the Maxwell Equations - microwave remote sensing has the radar equation. The radar equation relates the power transmitted to the power received for an active radar system. One form of the radar equation is

$$W_r = \frac{W_t G_t}{4\pi R^2} \sigma \frac{1}{4\pi R^2} A_r \qquad (2.2\text{-}1)$$

where:

W_r = received power

W_t = transmitted power

G_t = gain of transmitting antenna in direction of the target

R = range to the target

σ = effective backscatter area of the target

A_r = effective receiving area of the receive antenna.

The effective area of the receiving antenna is directly proportional to its gain times the square of the wavelength at which the antenna is operating:

$$A_r = \frac{G_r \lambda^2}{4\pi} \qquad (2.2\text{-}2)$$

Substituting (2.2-2) into (2.2-1) and collecting like terms yields

$$W_r = \frac{W_t G_t G_r \lambda^2 \sigma}{(4\pi)^3 R^4} \qquad (2.2\text{-}3)$$

A ground-sensing radar requires a somewhat modified form of Equation 2.2-3. Scatter of a radar signal from a ground target may usually be modeled by assuming that the individual scattering components of a resolution cell are sufficiently random so that each may be treated independently. With this assumption, phase considerations may be neglected and the return powers of each scattering component are added to obtain the total return power from the resolution cell [16]. Equation 2.2-3 assumes the form

$$W_r = \sum_{i=1}^{N} \frac{W_{ti} G_{ti} G_{ri} \lambda^2 \sigma_i}{(4\pi)^3 R_i^4} \qquad (2.2\text{-}4)$$

where:

N = the number of scatterers within the resolution cell

and i = identifies each scatterer with its respective illuminating power, antenna gains, and range.

Assuming that this resolution cell contains a large number of such scattering elements, the summation of Equation 2.2-4 may be replaced by an integral and the actual scattering cross-section for each individual area element may be replaced by the average value of scattering cross-section per unit area, σ° multiplied by the area A. This results in

$$W_r = \int_{\substack{\text{Scattering} \\ \text{Area}}} \frac{W_t G_t G_r \sigma^\circ \lambda^2 dA}{(4\pi)^3 R^4} \qquad (2.2\text{-}5)$$

where:

dA = differential element of ground area

σ° = scattering coefficient

The final step is to simplify Equation 2.2-5 by assuming that the total scattering area is small enough so that all of the terms except dA are constant and may be moved outside the integral sign. The integral of dA over the scattering area is just the area of the resolution cell, A_{ILL}. The radar equation for a ground target using these assumptions is

$$W_r = \frac{W_t G_t G_r \lambda^2 \sigma^\circ A_{ILL}}{(4\pi)^3 R^4} \qquad (2.2\text{-}6)$$

2.3 Scatterometer Calibration

The σ° equation results from the application of the radar equation for a ground target, Equation 2.2-6, to a radar scatterometer system during measurement of radar backscatter and calibration of the radar. Two types of calibration are necessary for a quantitative measurement of the amplitude of the backscatter return power.

Internal calibration may often be accomplished by injecting a sample of the transmitted signal into the receiver after it has passed through a delay line of fixed length and known attenuation.

Such a delay line is applicable to short range surface-based systems where the delay line may be comparable in length to the actual range of the system. This calibration produces a ratio of transmitted power to received power which is independent of short-term fluctuations of internal system parameters such as oscillator power variations, cable losses, mixer conversion losses, switch losses, and amplifier gains.

The internal calibration loop does not include the antennas or antenna cable, so any variations in this part of the system are not taken into account by the internal calibration. An external calibration is required to deal with these variations. A Luneberg-lens reflector is used here for this purpose. A Luneberg-lens reflector has a known scattering cross-section which has been measured in reference to a flat plate by the manufacturer. The frequency response of the lens used for this experiment* is shown in Figure 2.1.

A diagram of a simple radar scatterometer is shown in Figure 2.2. Constants indicating system loss parameters are labeled. The constant K includes losses from the transmitter to the transmit switch (S1) and from the receive switch (S2) to the receiver output.

The power at the output of the receiver during target observation is

$$W_{rt} = K_1 (K_t K_r) \frac{W_t G_t G_r \lambda^2 \sigma^0 A_{ILL}}{(4\pi)^3 R_t^4} \qquad (2.3\text{-}1)$$

*Serial Number 328, manufactured by Emerson and Cuming, Inc.

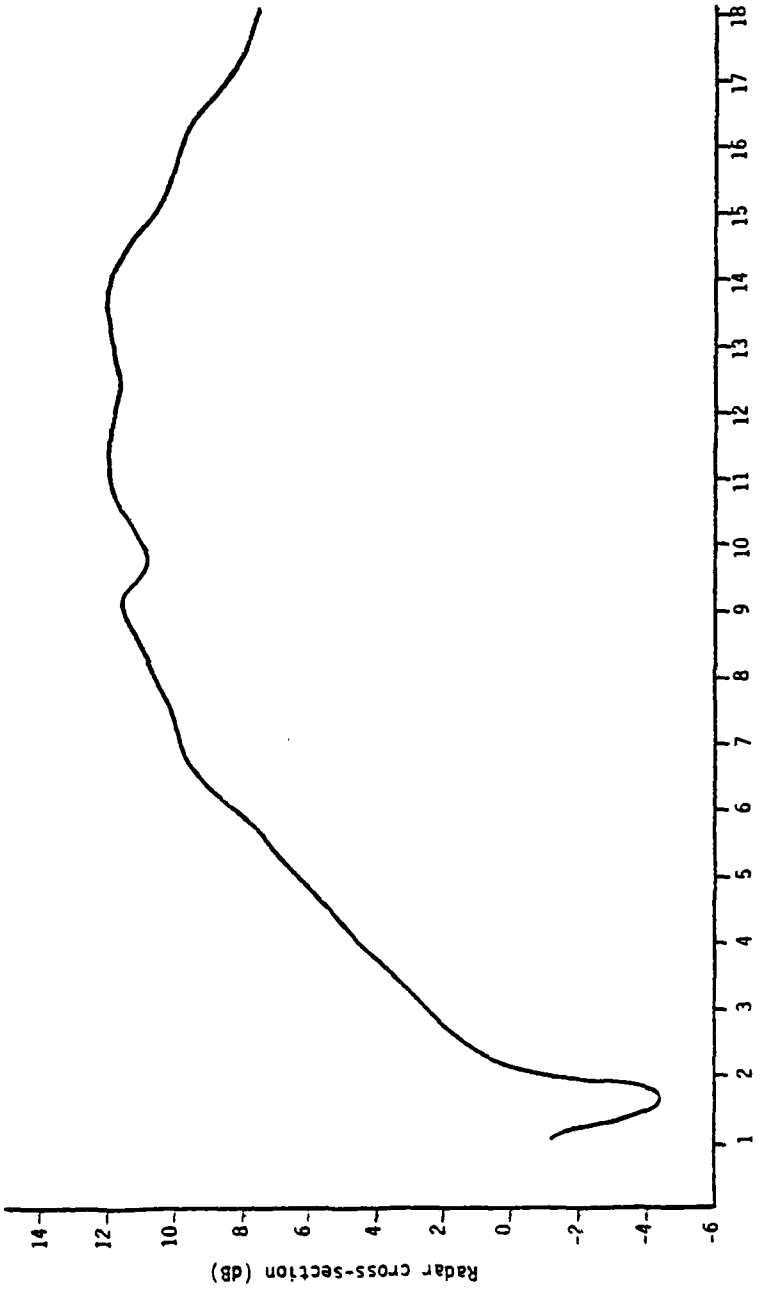

Figure 2.1: Frequency Response of Luneberg Lens Reflector

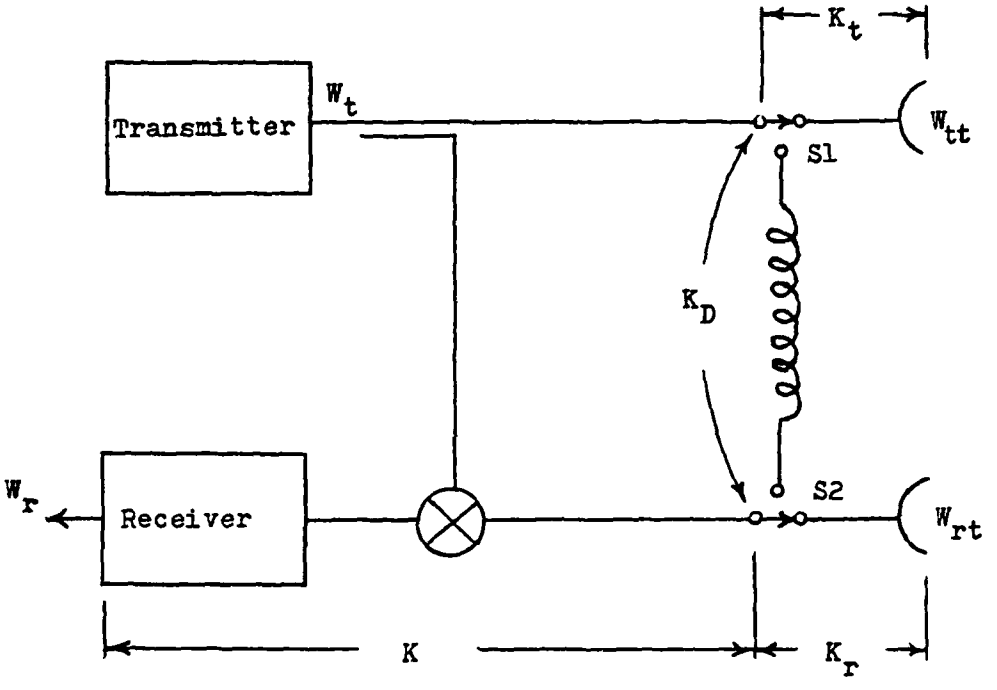

Figure 2.2

Simple Radar Scatterometer Indicating
System Loss Parameters

where:

W_{rt} = power return from target

K_1 = system loss during target measurement

R_t = range to target

Immediately after the target measurement is made a delay line measurement is done. The receiver output in this case is

$$W_{rDt} = K_1 W_t K_D \tag{2.3-2}$$

Taking the ratio of Equation 2.2-1 to 2.2-2 yields

$$\frac{W_{rt}}{W_{rDt}} = \left(\frac{K_t K_r}{K_D}\right)\left(\frac{G_t G_r \lambda^2}{(4\pi)^3}\right)\left(\frac{\sigma^o A_{LL}}{R_t^4}\right) \tag{2.3-3}$$

Notice this ratio is independent of the system variations represented by K_1 and the transmitter power W_t.

At some point during the experiment the external calibration using the Luneberg-lens reflector is done. The power at the receiver output during observation of the lens is

$$W_{rL} = K_2 (K_t K_r) \frac{W_t G_t G_r \lambda^2 \sigma_c}{(4\pi)^3 R_c^4} \tag{2.3-4}$$

where:

W_{rL} = power return from the lens

K_2 = system loss during lens measurement

R_c = range to calibration target (lens)

σ_c = scattering cross-section of the lens.

The power of the delay line reading taken immediately after the lens measurement is

$$W_{rDL} = K_2 W_t K_D \tag{2.3-5}$$

The ratio of Equations 2.3-4 and 2.3-5 yields

$$\frac{W_{rL}}{W_{rDL}} = \left(\frac{K_t K_r}{K_D}\right)\left(\frac{G_t G_r \lambda^2}{(4\pi)^3}\right)\left(\frac{\sigma_c}{R_c^4}\right) \tag{2.3-6}$$

Again notice the independence from K_2 and W_t.

Equations 2.3-3 and 2.3-6 may be combined and solved for σ^o. This result is

$$\sigma^o = \left(\frac{W_{rt}}{W_{rDt}}\right)\left(\frac{W_{rDL}}{W_{rL}}\right)\left(\frac{\sigma_c R_t^4}{A_{ILL} R_c^4}\right) \tag{2.3-7}$$

This equation for σ^o may be written in decibels as:

$$\begin{aligned}\sigma^o &= W_{rt}(dB) - W_{rDt}(dB) + W_{rDL}(dB) - W_{rL}(dB) \\ &\quad + \sigma_c(dB) - 10 \log_{10} A_{ILL} + 40 \log_{10} R_t - 40 \log_{10} R_c.\end{aligned} \tag{2.3-8}$$

Equation 2.3-8 is the σ^o equation for the radar scatterometer. The first four terms are measured directly by the system, the σ_c term is obtained from the manufacturer's data, and the last three terms are determined by the location of the target. Normally the lens is positioned so that $R_t = R_c$.

The range to the target (R_t) is available from the system geometry of Figure 2.3. Range is related to height of the antennas by

$$R_t = \frac{h}{\cos\theta} \tag{2.3-9}$$

where:

h = height of antennas

θ = angle of incidence.

The range to target for the surface-based scatterometer system remains constant while h varies as the structure is adjusted to alter incidence angle. For the helicopter-borne scatterometer system h is measured with a radar altimeter and R_t is calculated using Equation 2.3-9.

The radar scatterometer used in this experiment is a frequency-modulated continuous-wave (FM-CW) system. A relationship between range to target and the transmitter parameters exists for this type of system. This relationship is found by comparing similar triangles ABC and ADE shown in Figure 2.4.

$$\frac{\Delta F}{\frac{1}{2F_m}} = \frac{F_{if}}{\frac{2R}{c}} \tag{2.3-10}$$

Rearranging terms gives

$$R = \frac{c\,F_{if}}{4\,F_m\,\Delta F} \tag{2.3-11}$$

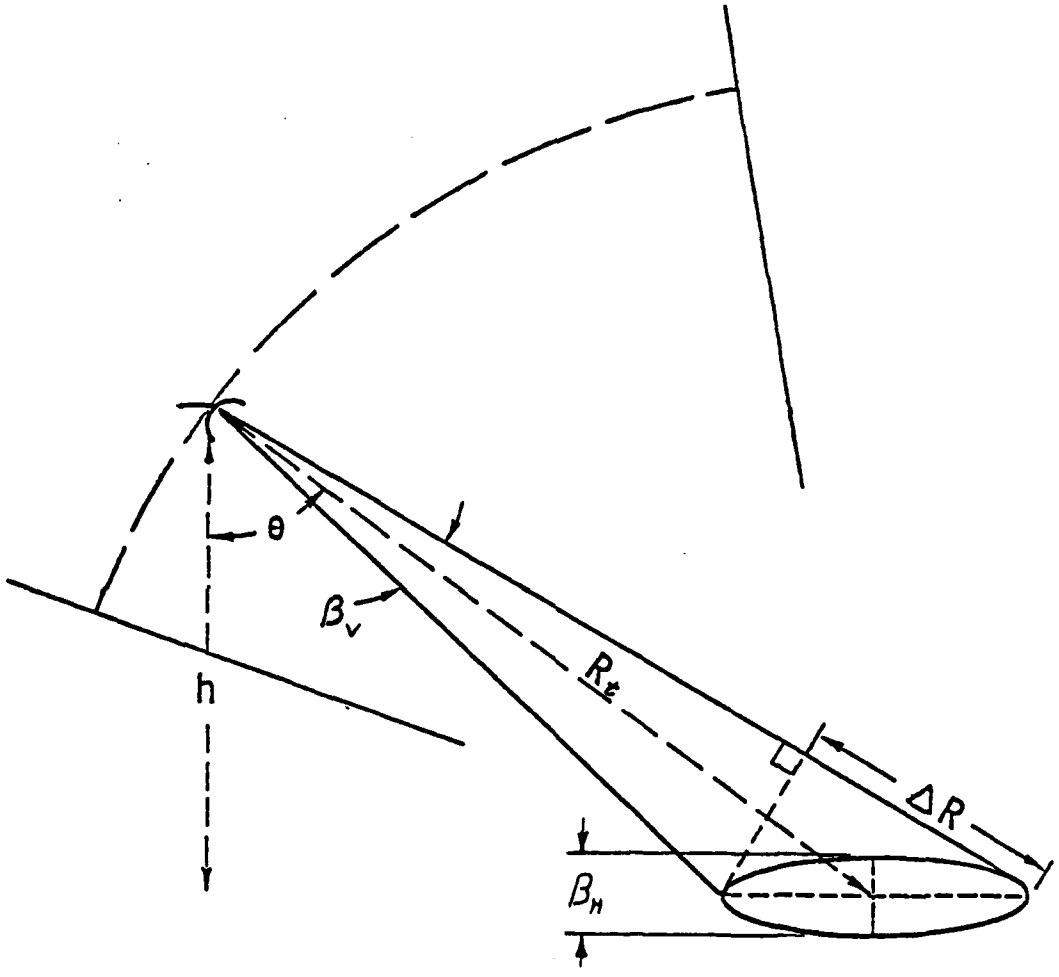

Figure 2.3
Radar System Geometry

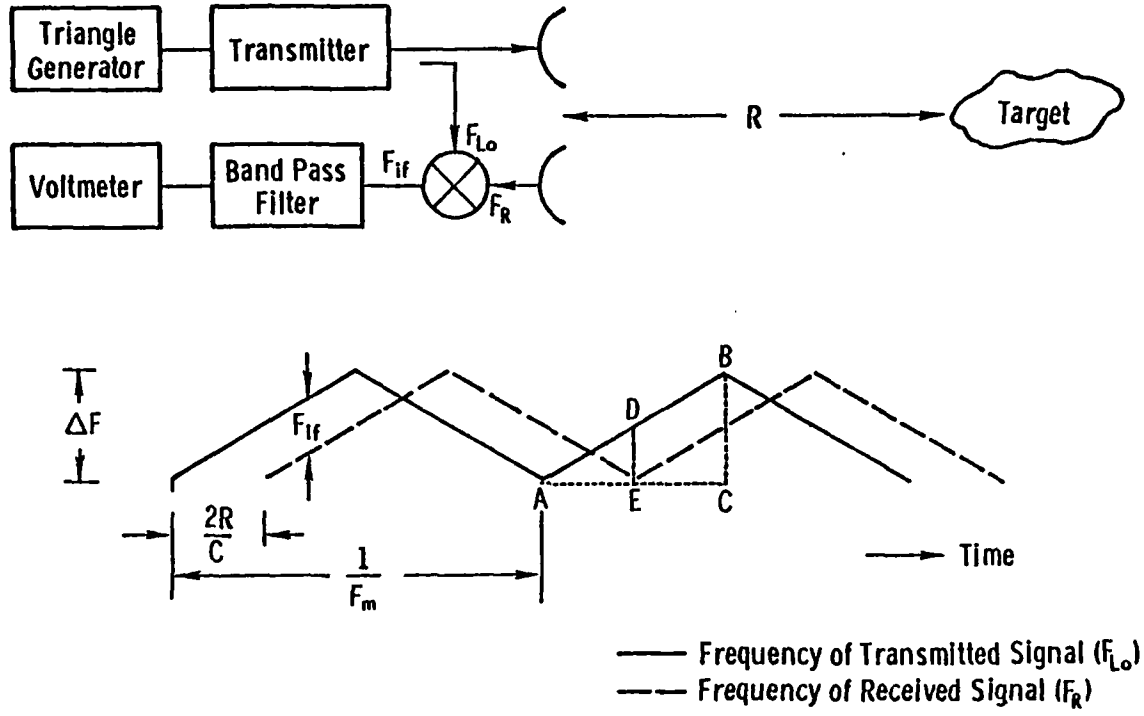

Figure 2.4: Simplified FM-CW System

where:

R = range to target

c = velocity of propagation

F_{if} = intermediate frequency

F_m = modulation rate

ΔF = F_m sweep deviation.

Equation 2.3-11 may be used to compute range if the modulation rate is known and conversely may compute the proper modulation rate given the range.

2.4 Calculation of Illuminated Area

Accurate calculation of illuminated area, A_{ILL}, is important for an accurate estimate of the scattering coefficient. A_{ILL} is determined from the geometry of Figure 2.3 and, with knowledge of the effective gain-product antenna patterns, for the system. It is assumed that the antenna beam interaction with the ground is an ellipse with semi-major and semi-minor axes a and b, given by

$$a = \frac{R_t}{2} \cos\theta \left[\tan\left(\theta + \frac{\beta_v}{2}\right) - \tan\left(\theta - \frac{\beta_v}{2}\right)\right] \qquad (2.4\text{-}1)$$

$$b = R_t \tan\frac{\beta_H}{2} \qquad (2.4\text{-}2)$$

where:

R_t = range to the target at the beam center

θ = incidence angle at beam center

β_v = elevation plane effective gain product 3 dB beamwidth

β_H = azimuth plane effective gain product 3 dB beamwidth.

The illuminated area is

$$A_{ILL} = \pi a b$$

$$= \frac{\pi R_t^2}{2} \tan\frac{\beta_H}{2} \cos\theta\left[\tan\left(\theta+\frac{\beta_V}{2}\right) - \tan\left(\theta-\frac{\beta_V}{2}\right)\right] \qquad (2.4\text{-}3)$$

Accurate measurement of the antenna beamwidths is very critical if the illuminated area calculation is to be accurate. Difficulties in obtaining precise antenna characteristics create uncertainty in the estimate of σ^o. Fortunately antenna characteristics are stable for long periods of time so measurements made with the same system are accurate with respect to each other. Only fading presents a greater problem than the antenna characteristics. Fading will be discussed shortly.

Equation 2.4-3 is only applicable if the radar system is operating under beamwidth-limited conditions. Referring again to Figure 2.3, it is seen that, when the resolution cell is defined by the beamwidth, the range resolution ΔR, is given as

$$\Delta R = h\left[\sec\left(\theta+\frac{\beta_V}{2}\right) - \sec\left(\theta-\frac{\beta_V}{2}\right)\right] \qquad (2.4\text{-}4)$$

The other condition applicable to an FM radar system is filter (range) limiting. For the filter-limiting case the range resolution is

$$\Delta R = R_t \frac{\Delta F_{if}}{F_{if}} \qquad (2.4\text{-}5)$$

where:

ΔF_{if} = effective bandwidth of the IF bandpass filter

F_{if} = intermediate frequency.

For cases where the range resolution of Equation 2.4-4 is less than that of 2.4-5 the radar system is operating under beamwidth limiting conditions. If filter limiting becomes applicable, ΔR of (2.4-5) greater than that of (2.4-4), the ground pattern is no longer an elipse and corrections must be made in order to obtain an accurate illuminated area.

2.5 *Fading*

Fading was mentioned earlier as the greatest source of uncertainty in the estimate of the scattering coefficient. Fading results from the constructive and destructive interference of the signal components originating from the individual scattering elements of the resolution area. The measured power thus varies in amplitude or fades in and out.

Effects of fading may be reduced by averaging large numbers of independent samples. Spatial averaging and frequency averaging are two methods of obtaining additional independent samples. Spatial averaging is accomplished by observing more than one area of the target surface and averaging the measurements. Frequency averaging, or the use of excess system bandwidth, also produces additional independent samples. For this technique, the resolution bandwidth or frequency separation between independent samples is given by [17]

$$\Delta F_r = \frac{150}{D} \quad MHz \qquad (2.5\text{-}1)$$

where:

ΔF_r = resolution bandwidth

D = maximum range variation across the resolution cell (meters).

ΔF_r is the minimum bandwidth required in order to resolve a sample. Any additional or excess bandwidth results in additional independent samples. The number of independent samples N_f obtained through use of excess bandwidth or frequency averaging is

$$N_f = \frac{\Delta F}{\Delta F_r} \qquad (2.5\text{-}2)$$

2.6 Sensor Description

The sensor used in this measurement program is a multi-frequency, multi-polarization, and multi-angle of incidence frequency-modulated continuous-wave (FM-CW) radar scatterometer. The frequency range covered includes L-band (1-2 GHz) and Ku-X-band (8-18 GHz). Polarization capabilities include HH, HV, VV and VH (H = horizontal, V = vertical; the first letter identifies transmitted polarization and the second identifies received polarization). Angles of incidence are selectable between 10° and 75° (measured with respect to vertical).

Two different operating configurations are available with this sensor. A surface-based TRAMAS system and a helicopter-mounted HELOSCAT system were each designed to fulfill different needs. These systems are discussed fully in the next two sections. A block diagram which is applicable to both systems appears in Figure 2.5.

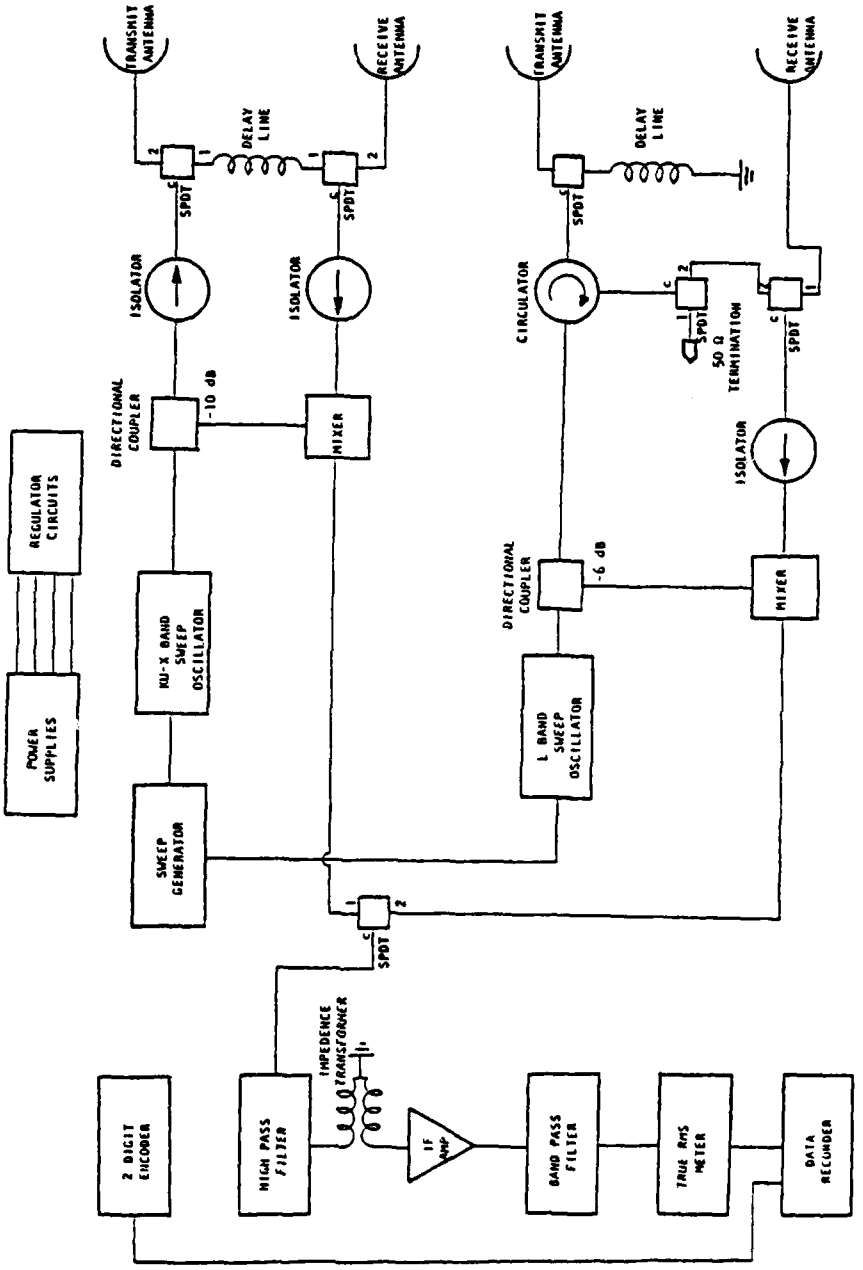

Figure 2.5: RF Block Diagram

Circuits in the sweep generator block of this diagram produce a triangular modulation waveform which is directed to the sweep oscillators. The L-band oscillator is swept from 1.1 to 1.9 GHz. The Ku-X-band oscillator is swept across a 1 GHz band with center frequencies at 9.0, 10.0, 11.0, ..., and 17.0 GHz.

Internal calibration of the radar is accomplished with delay lines which have lengths comparable to the range to target for the system. The delay line is switched between the transmit and receive ports of the Ku-X-band section. A short-circuited delay line is used in the L-band section and is switched into the transmit port during calibration. External calibration consists of measuring the back-scatter from a Luneberg-lens reflector which is a standard radar target of known cross-section.

The impedance transformer shown between the high pass filter and the intermediate frequency (IF) amplifier improves the signal-to-noise characteristics of the sensor. Data is recorded on a paper tape printer. Recent modifications of the system include a micro-processor controller which has automated many of the manual operations required with the original system. Included is the replacement of the paper tape printer with a cassette tape recorder.

2.6.1 The TRAMAS System

The Transportable Microwave Active Spectrometer, TRAMAS, system is a four antenna FM-CW scatterometer mounted on a portable surface-based structure. The structure was designed so that it could be transported to and from ice sites with a snowmobile and sled, heli-copter, or small aircraft. The distance to ice sites investigated

during March 1979 at Tuktoyaktuk required that the structure be slung between sites with a helicopter. This operation is illustrated in Figure 2.6.

Figure 2.7 shows the TRAMAS system erected on the ice during an experiment. The dish and horn antennas of the L-band radar are located at the apex of the structure. VV and VH polarizations are obtained by rotating the dish antenna. The two dish antennas of the Ku-X-band system are mounted at the base of one leg of the structure and point at the flat plate reflector located on the opposite leg. HH, HV, VV and VH polarizations are available with this system. Angles of incidence between 10° and 75° are selectable with the structure. The range to the target remains constant for both the L-band and the Ku-X-band radars as the angle of incidence is varied. Complete system specifications are provided in Table 2.1.

The TRAMAS system has the advantage of having a well-defined footprint on the target surface. This makes the collection of surface-truth information at the time of backscatter measurements a very simple matter. This footprint remains fixed on the same area of the target as long as the structure is not moved. This feature is useful for making long-term measurements, such as the effects of solar heating or ambient temperature variations.

Two major disadvantages of the TRAMAS system are (1) that it requires a fairly smooth and level surface to operate on, and (2) that set-up and tear-down are very time consuming. This limits the system to thick and thin first-year, multiyear, and lake ice types. Rubble fields and large pressure ridges are very difficult to study with this system.

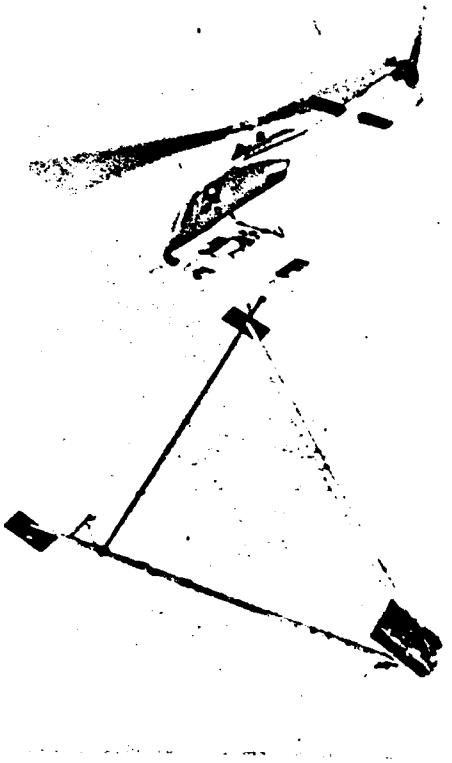

Figure 2.6: TRAMAS Structure Being Slung to an Ice Site (March 1979)

Figure 2.7: TRAMAS System During an Experiment (March 1979)

TABLE 2.1

NOMINAL SYSTEM SPECIFICATIONS - TRAMAS

	Ku X-band	L-band
Type	FM-CW	FM-CW
Frequency Range	8-18 GHz	1.5 GHz
Modulating Waveform	Triangular	Triangular
FM Sweep: ΔF	1.0 GHz	800 MHz
Transmitter Power	14-19 dBm	19 dBm
Intermediate Frequency	50 kHz	50 kHz
IF Bandwidth	13.5 kHz	13.5 kHz
Antennas:		
Receive Type	46 cm. Reflector	91 cm. Reflector
Transmit Type	31 cm. Reflector	Standard Gain Horn
Feeds	Dual Ridge Horn	Log Periodic
Polarization Capabilities	HH, HV, VV, VH	VV, VH
Transmit Beamwidth	8.2° at 8 GHz 4.0° at 17.7 GHz	27°
Receive Beamwidth	5.3° at 8 GHz 2.3° at 17.8 GHz	9.5°
Target Distance	10.9 meters	6.5 meters
Incidence Angle Range	10° - 75°	10° - 75°
Calibration		
Internal	Signal Injection (delay line)	Signal Injection (shorted delay line)
External	Luneberg Lens Reflector	Luneberg Lens Reflector
Operating Temperature Range	-50°C to +50°C	-50°C to +50°C

2.6.2 The HELOSCAT System

The HELOSCAT system was originally designed to accommodate both the L-band and Ku-X-band radars with an external support for four antennas. This experiment utilized only the Ku-X-band radar with its two small dish antennas. The HELOSCAT system is limited to angles of incidence of 20°, 40°, and 60° and to VV polarization. Complete system specifications are given in Table 2.2.

A Bell model 205 helicopter was used as the platform for this system. The external components of the system, the antenna structure and the radar altimeter, are attached to the helicopter using external stores rack auxiliary kits (Bell Helicopter No. 205-706-013). The internal configuration of the HELOSCAT system is diagrammed in Figure 2.8, and Figure 2.9 shows the antenna structure mounted on the helicopter.

All electronics for the system except the RF hardware box and the static inverter were contained in the equipment rack. The RF box was located as close as possible to the antenna structure to minimize the length of the antenna cables. The static inverter is a device which converts the aircraft 28 VDC into 120 VAC at 60 Hz for the radar system. It was positioned beneath the seat of crew member number 2.

Crew member number 1 was responsible for the operation of the radar system. Crew member number 2 recorded the altitude and the FM frequency for each data point and kept notes on the data procedure. Crew member number 3 was in communication with the pilot and also kept notes on the ice type, site location, and surface conditions.

A photograph of the HELOSCAT system during external calibration with the Luneberg-lens is shown in Figure 2.10. The antennas are

TABLE 2.2

NOMINAL SYSTEM SPECIFICATIONS -- HELOSCAT

	Ku X-band
Type	FM-CW
Frequency Range	8-18 GHz
Modulating Waveform	Triangular
FM Sweep: Δf	1.0 GHz
Transmitter Power	14-19 dBm
Intermediate Frequency	50 kHz
IF Filter Bandwidth	13.5 kHz
Antennas:	
Receive Type	46 cm. Reflector
Transmit Type	31 cm. Reflector
Feeds	Dual Ridge Horn
Polarization Capability	VV
Transmit Beamwidth	8.2° at 8 GHz 4.0° at 17.7 GHz
Receive Beamwidth	5.3° at 8 GHz 2.3° at 17.8 GHz
Incidence Angles Available	20°, 40° and 60°
Calibration:	
Internal	Signal Injection (delay line)
External	Luneberg Lens Reflector
Operating Temperature Range	-50°C to +50°C
Helicopter Attitude	Hover at 50 feet

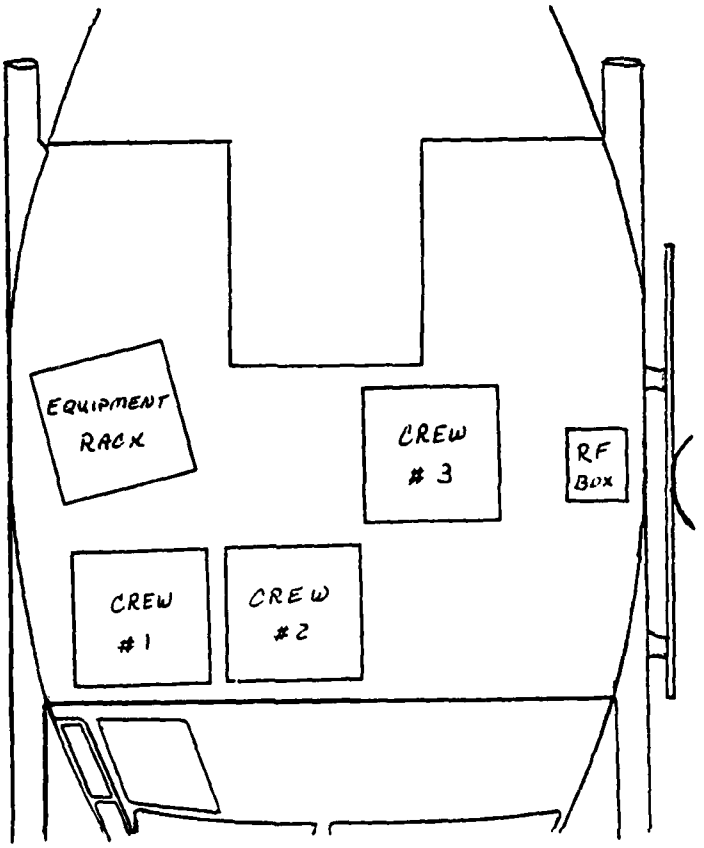

Figure 2.8

Internal Configuration of HELOSCAT System
(March 1979)

Figure 2.9: HELOSCAT Antenna Structure Mounted on Bell 205 Helicopter (March 1979)

Figure 2.10: HELOSCAT System External Calibration (March 1979)

focused at a range which corresponds to the range for the 40° incident angle and a one hundred foot altitude. The external calibration is also done at this range.

The disadvantage of only a single polarization and a limited number of incidence angles is easily compensated for by the mobility of the HELOSCAT system. A wide variety of ice types can be investigated in a day's time as contrasted with the TRAMAS system which requires 3-4 hours at each site just for assembly and disassembly. Such features as rubble fields and pressure ridges present no problem for the HELOSCAT system.

3.0 EXPERIMENT DESCRIPTION

3.1 Background

The March 1979 Arctic expedition of the University of Kansas Sea Ice Group was conducted as a part of the Beaufort Sea Ice Experiment segment of the Canadian SURSAT (Surveillance Satellite) Project. Facilities and support equipment of the Canadian Polar Continental Shelf Project (PCSP) base camp were made available to the experiment groups participating in the project. The PCSP base camp is located at Tuktoyaktuk, N.W.T., Canada. A map showing the location of Tuktoyaktuk and some of the area surrounding it is shown in Figure 3.1.

The purpose of the Beaufort Sea Ice Experiment segment of the SURSAT Project was to conduct detailed investigations of the sea ice off the Canadian coast near Tuktoyaktuk. Information acquired as a part of these investigations was intended to complement data obtained through observations of the area with sensors aboard the SEASAT-A satellite. Unfortunately, the satellite suffered a catastrophic failure before the SURSAT experiments occurred. Participants in the SURSAT Project included research teams from university and government agencies of Canada and the United States and personnel from several oil companies.

A summary of the backscatter measurements made by the University of Kansas research group is presented in Table 3.1. Four different types of ice were investigated as a part of this experiment including fresh-water inland lake ice, thin first-year sea ice, thick first-year sea ice, and brackish sea ice. It had been hoped that multiyear sea ice would be available for investigation as a part of the experiment

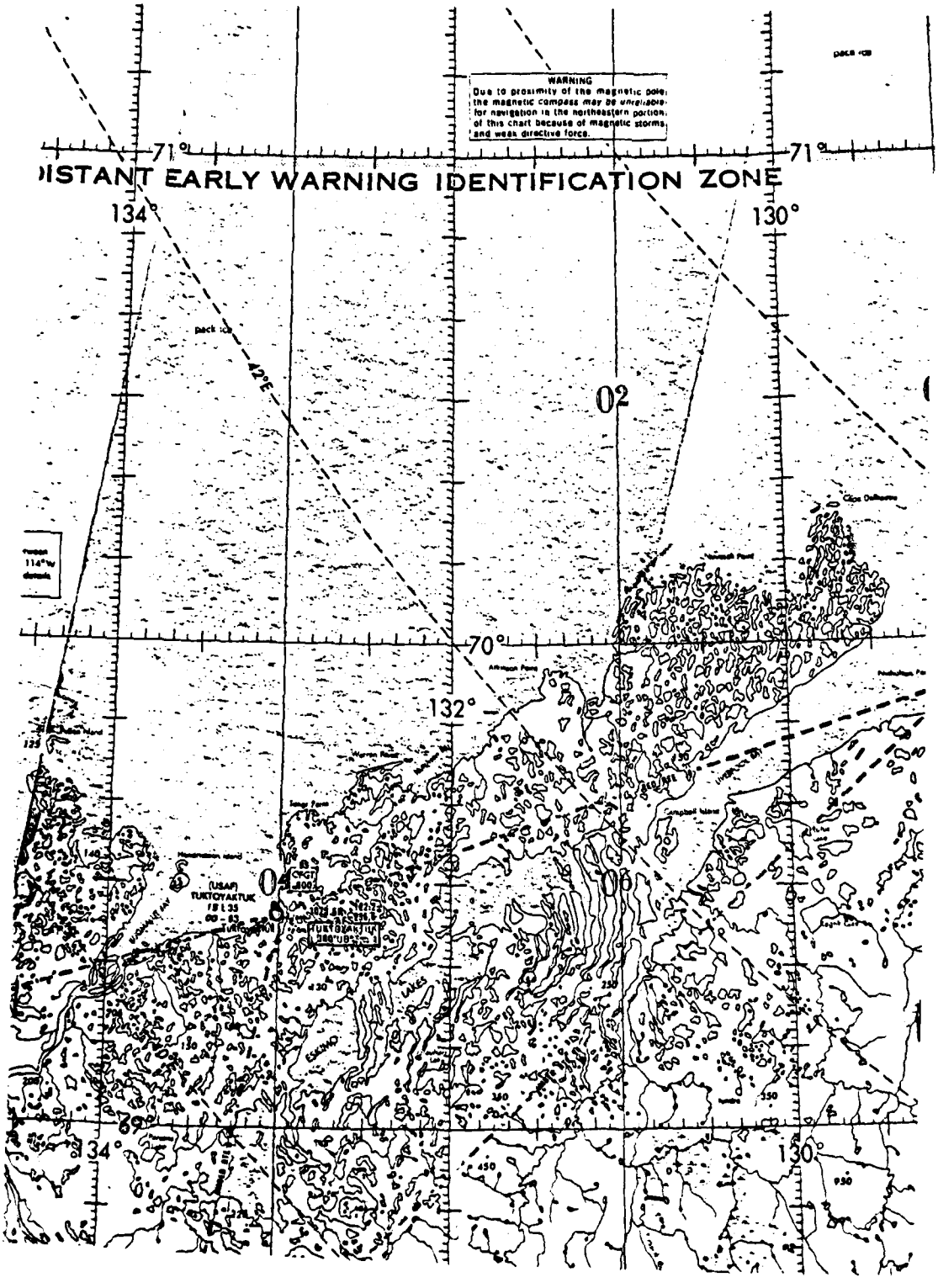

Figure 3.1: Map of Experiment Area (March 1979)

TABLE 3.1

SUMMARY OF BACKSCATTER MEASUREMENTS

Sensor	Date	Site Number	Ice Type	Number of Looks
TRAMAS	3/13	T1	Lake	2
	3/14	T2	Thick FY	3
	3/15	T3	Thick FY	4
	3/16	T4	Thin FY	3
	3/21	T5	Lake	5
HELOSCAT	3/31	H1	Lake	10
	4/1	H2	Lake	10
	4/1	H3	Brackish	13
	4/1	H4	Thick FY	10
	4/1	H5	Thick FY	10
	4/1	H6	Thick FY	10
	4/1	H7	Thin FY	15
	4/1	H8	Brackish	14

but the nearest multiyear ice floes were located well out in the pack ice, several hours helicopter flight time away from Tuktoyaktuk. Plans were made to conduct investigations at one of these ice sites with the HELOSCAT system. Poor weather and reliability problems with the radar forced the cancellation of that part of the experiment.

3.2 Procedures

Initial set-up and testing of the TRAMAS system was done on a small pond located immediately adjacent to the PCSP base camp. Measurements were made with HH, VV and HV polarizations and fourteen angles of incidence from 10° to 75°. The extremely cold (-30° C) conditions created some problems with the portable generator that was used to provide power for the system. The generator had to be protected from the wind and if the motor ever stopped it had to be restarted within a minute, or it could not be restarted until it had been warmed up. The system electronics, which are specified to -50° C, performed admirably.

Once system testing and investigation of the lake ice was completed, a Bell model 206 helicopter provided by PCSP for project support was used to sling the structure to a thick first-year ice site. Two days were spent investigating this site. The three-person experiment team was ferried out to the site each morning by the helicopter and picked up approximately seven hours later and returned to the base camp. Survival equipment, which included a tent, sleeping bags, heater, gun, and emergency radio, were always kept at the site with the experimenters.

The system was next moved to a thin first-year sea ice site a few miles from the thick first-year site. The experiment at this site

was interrupted during its second day by a breakup of the ice. Following a retreat from this site the system was returned to the lake ice site and the TRAMAS portion of the experiment was completed.

The HELOSCAT experiment began with a trip to Inuvik, N.W.T., Canada, to install the HELOSCAT system on a Bell model 205 helicopter. Flight tests were conducted at Inuvik to obtain a certification from the Canadian Ministry of Transport (MOT). Four types of ice were investigated with the HELOSCAT system. Studies of the lake, thin first-year, and thick first-year sites investigated with the TRAMAS system were conducted, and a brackish sea ice site was studied. Brackish ice is formed where a river empties into the ocean, creating a mixture of low salinity river water and sea water.

Results of a test the first morning of the HELOSCAT experiment prompted a decision to operate the HELOSCAT system at an altitude of fifty feet. The system sensitivity was determined to be significantly better at the fifty foot altitude than at the 100 foot altitude which had been used previously during the April 1978 experiment at Point Barrow, Alaska.

During the operation of the HELOSCAT system each member of the three man experiment team had a specific task to perform. One was responsible for the operation of the radar. Magnitude of the back-scatter return was peaked by adjustment of a potentiometer which controls the FM frequency. Several data samples were recorded and the procedure was then repeated for the next frequency setting. Recent addition of a phase-lock loop tracking circuit which centers the return power spectrum in the passband of the IF filter will eliminate this

manual operation in the future. The second crew member recorded the altitude and the FM frequency associated with each data set and made notes related to the data-taking procedure, while the third member was in communication with the pilot and recorded observations about the ice conditions and site locations.

3.3 Surface-Truth

Surface-truth measurements of a target being investigated are important if one wishes to correlate changes in the physical properties of the target with changes in the backscatter response. This information is important also if one attempts to compare with responses from similar ice types of the same experiment or results from prior experiments. Surface-truth measurements should always include the following information:

1. Classification of ice type
2. Air Temperature
3. Air-snow interface temperature
4. Snow depth
5. Snow-ice interface temperature
6. Ice thickness
7. Description of surface conditions -- both large and small scale.

Figure 3.2 shows experiment personnel using an ice auger to measure ice thickness. A more detailed analysis of the target would include the following measurements in addition to those listed above:

1. Ice salinity profile
2. Description of vertical inhomogeneities (visual core examination)

Figure 3.2: Experiment Personnel Making Measurement of Ice Thickness (March 1979)

3. Description of horizontal inhomogeneities (thin sections of ice cores)
4. Ice temperature profile
5. Ice density
6. Snow density
7. Snow wetness
8. Preferred crystal orientation.

The research teams that participated in the SURSAT experiment at Tuktoyaktuk attempted to study the same ice sites so that comparisons of results would be meaningful and to eliminate duplication of surface-truth efforts. Several of the groups were responsible for extensive surface-truth measurements that were to be shared with the other groups. The University of Kansas team concentrated on making backscatter measurements and performed only minimal surface-truth measurements of temperatures and description of the surface conditions. Ice surface temperatures ranged from -20° to -28° C. Air temperatures throughout the experiment were about -30° C.

The thick first-year sea ice site was designated Site A by the experimenters. This relatively large floe had a very smooth flat surface with minimal snow cover. Ice thickness was approximately 1.3 meters. The floe was located at 70° 00' N and 132° 00' W, about 45 miles northeast of Tuktoyaktuk (refer to the map of Figure 3.1). The floe was very close to the edge of the ice shear zone at that time.

The thin first-year sea ice site was located a few miles to the north of Site A near a refrozen lead in the shear zone. The surface of this ice was covered with salt flowers as illustrated in Figure 3.3.

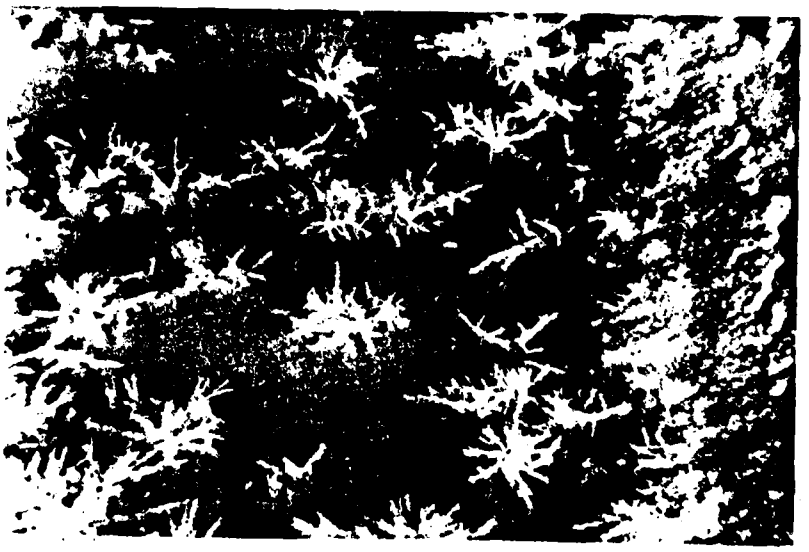

Figure 3.3: Salt Flowers at Thin First-Year Sea Ice Site (March 1979)

These crystalline formations have a very high salinity (87 °/₀₀) compared to that of the ice surface (15 °/₀₀).

The fresh-water lake ice site was a small pond located on the opposite side of the main road adjacent to the PCSP base camp. This site is referred to as the PCSP pond. The lake is 180 cm deep and was frozen completely to the bottom. The surface was covered by a rough snow cover that varied from 2-8 cm in depth.

The brackish sea ice site was located just off-shore to the southwest of the PCSP base camp. This site was studied with the HELOSCAT system only. The ice surface had a heavy drifted snow cover.

A comparison of salinity profiles for thin first-year, thick first-year, and multiyear sea ice is presented in Figure 3.4. The thin first-year ice has the highest overall salinity, particularly at the surface due to the salt flowers. The profile for thick first-year ice indicates a high salinity at the surface which decreases with depth. Data were not available for depths below 100 cm, but if it had been it would have indicated that salinity again increases as the ice-sea water interface is approached. This is characteristic of salinity profiles for thick first-year ice. The multiyear ice has a very low salinity at the surface which steadily increases with increasing depth. Of course, the fresh-water lake ice site investigated had a very low salinity at all depths.

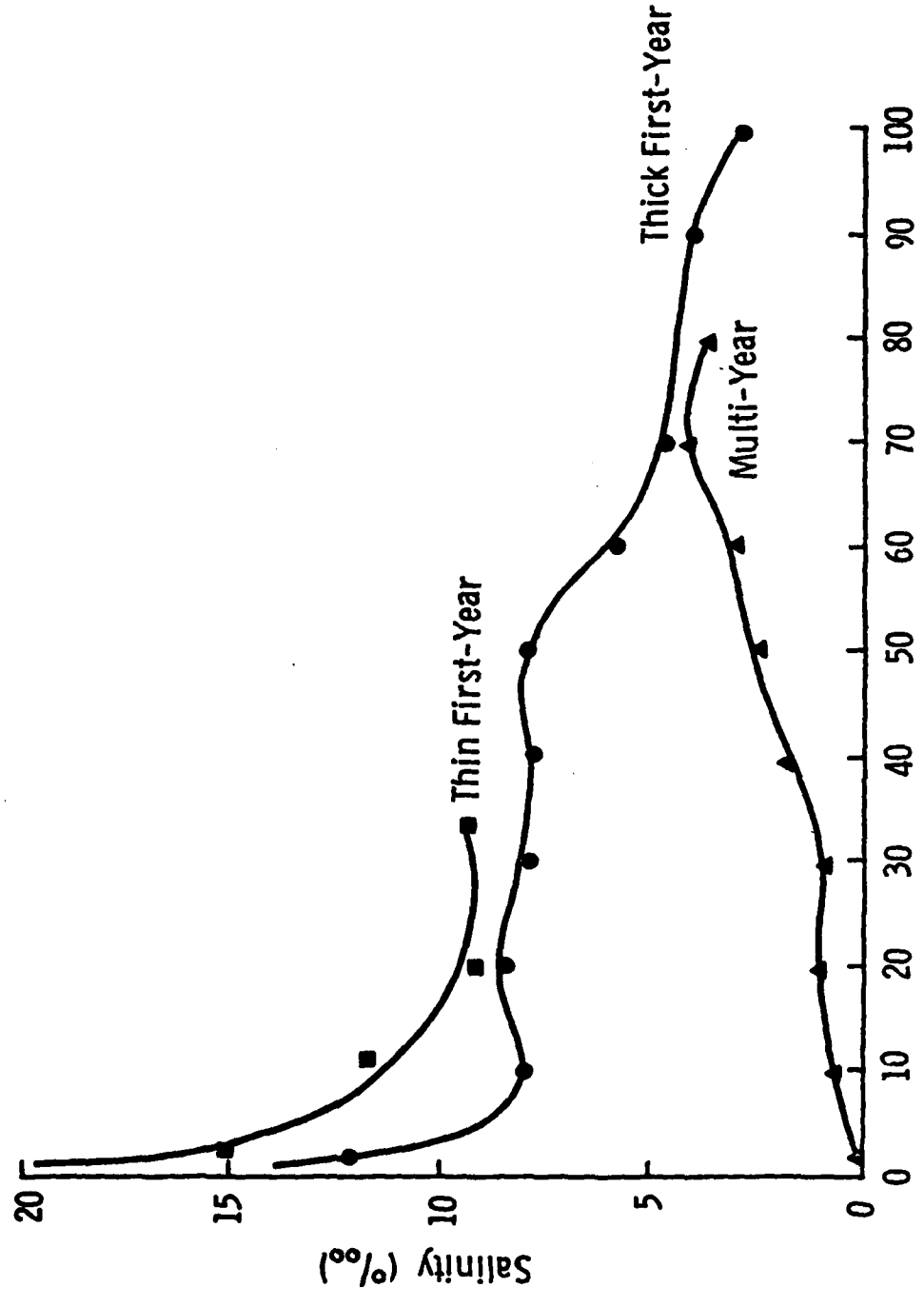

Figure 3.4: Salinity Profiles of Thin First-Year, Thick First-Year, and Multi-Year Sea Ice (March 1979)

4.0 MARCH 1979 EXPERIMENT RESULTS

Results of the March 1979 experiment at Tuktoyaktuk are presented in this chapter. Scattering coefficients obtained with the L-band and the Ku-X-band TRAMAS system are discussed in the first two sections. The next section presents the results of the HELOSCAT system experiment which was conducted at the Ku-X-band frequencies. This is followed by a comparison of the TRAMAS system results with those of the HELOSCAT system for the Ku-X-band frequencies.

4.1 L-Band TRAMAS Results

Graphs of the average scattering coefficient versus angle of incidence for the data obtained with the L-band radar are shown in Figures 4.1 and 4.2. The trend lines of the thick first-year and thin first-year sea ice are nearly identical for vertical polarization indicating little or no discrimination capability. The cross-polarization trends separate significantly for incidence angles greater than 40° with scattering from thick first-year above that from thin first-year sea ice demonstrating an ability to discriminate these types of ice for these conditions. Lake ice may be distinguished from thick and thin first-year sea ice for incidence angles between 20° and 60°. No lake ice data were available for the VH polarization at this frequency. Although L-band does not show much promise for discrimination applications, L-band imaging radars have been demonstrated to be useful for topographic mapping applications.

4.2 Ku-X-Band TRAMAS Results

Scattering coefficient trends of thick first-year sea ice, thin first-year sea ice, and fresh-water lake ice for 9, 13, and 17 GHz and

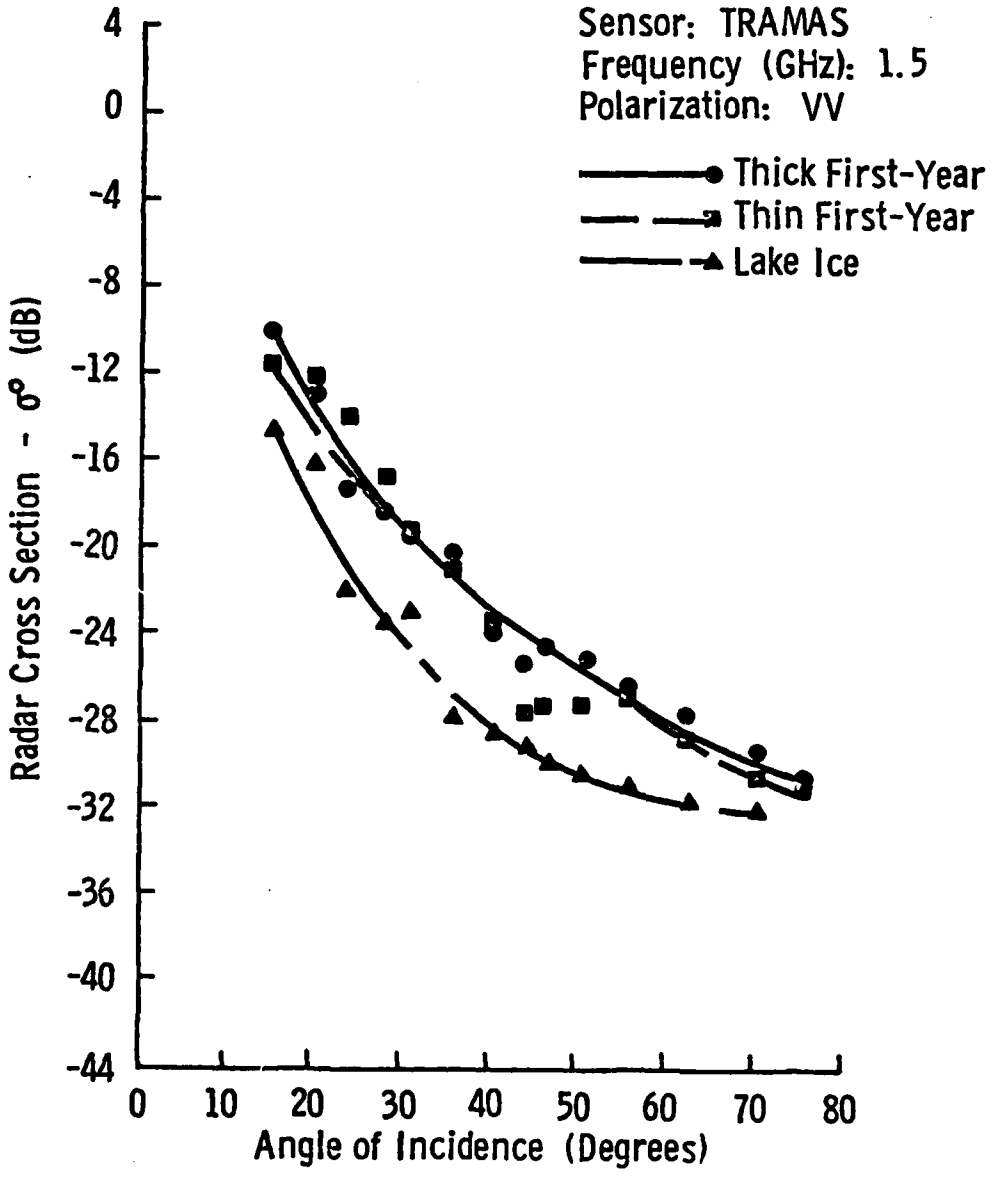

Figure 4.1: Average Scattering Coefficient of Thick First-Year, Thin First-Year, and Lake Ice at 1.5 GHz (March 1979)

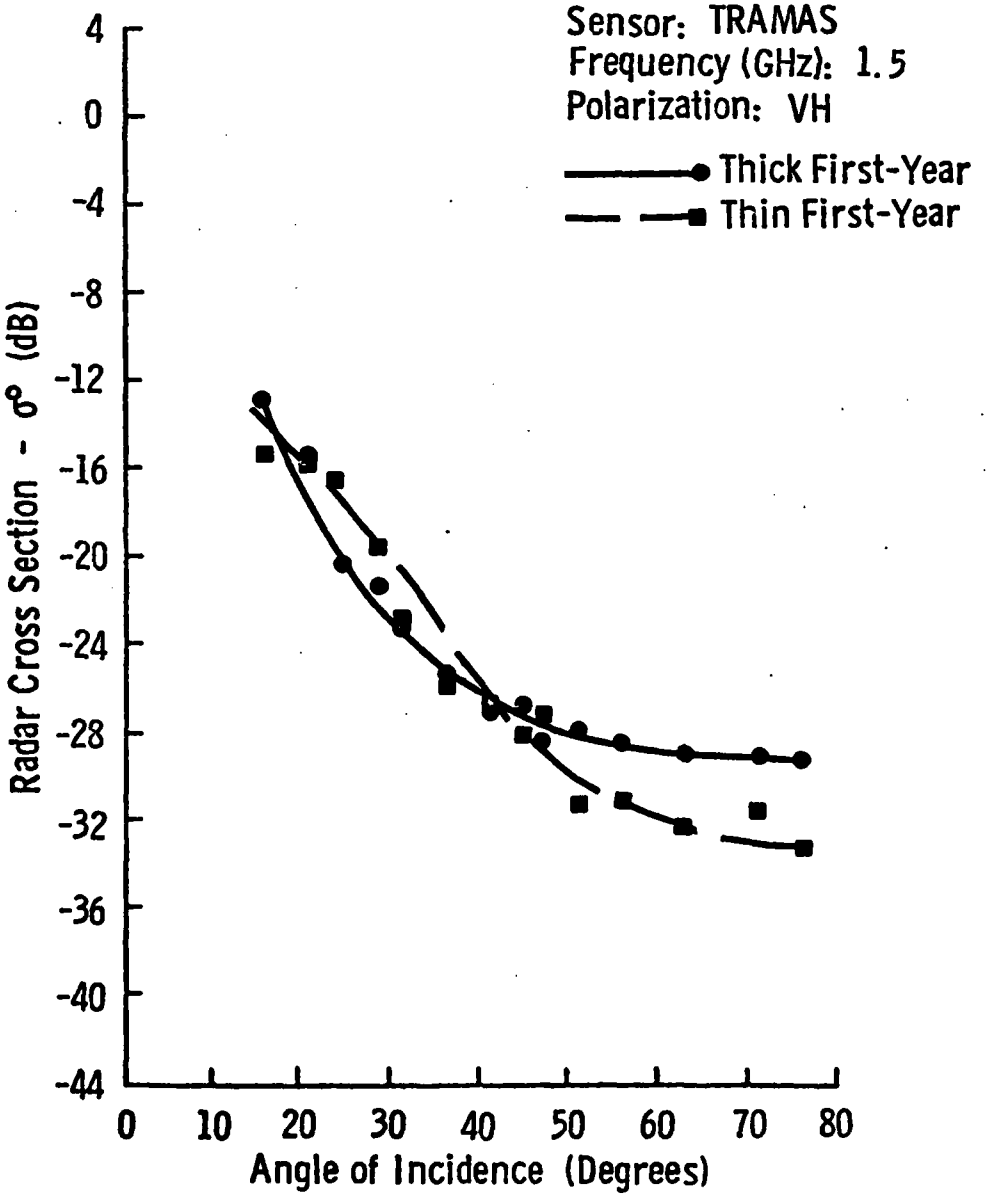

Figure 4.2: Average Scattering Coefficient of Thick First-Year and Thin First-Year Sea Ice at 1.5 GHz (March 1979)

various polarizations are shown in Figures 4.3 through 4.9. Discrimination between these three ice types may be possible with selection of the proper incidence angle. This conclusion applies for all frequencies in the 8-18 GHz region. Figures 4.3, 4.4 and 4.5 show that each polarization (VV, HH and HV) also has the ability to discriminate among these ice types.

In each case lake ice has the lowest scattering coefficient and may easily be discriminated from the two thick first-year sea ice types. This observation is true for all incidence angles except those near nadir. The scattering coefficient trends for thick and thin first-year sea ice demonstrate parallel angular responses for a large number of cases. Angles of incidence between 10° and 70° would provide discrimination in these cases.

Figure 4.10 shows the ability to distinguish between thick first-year sea ice, thin first-year sea ice, and lake ice for vertical polarization as a function of frequency, angle of incidence, and decibel difference of the σ^{o} values for these ice types. There is very little ability to discriminate thick from thin ice at 1.5 GHz. The other frequencies all indicate similar differences between thick and thin ice. The best discrimination capability occurs for angles of incidence greater than 40°. Figure 4.11 shows that all of the frequencies have the ability to distinguish thick first-year sea ice from lake ice at almost all angles of incidence. Larger incidence angles again are associated with the greatest differences, particularly for the 9 GHz frequency. The separation between ice types is seen to decrease for frequencies in the 8-18 GHz region. These observations lead to the conclusion that the best discrimination capability

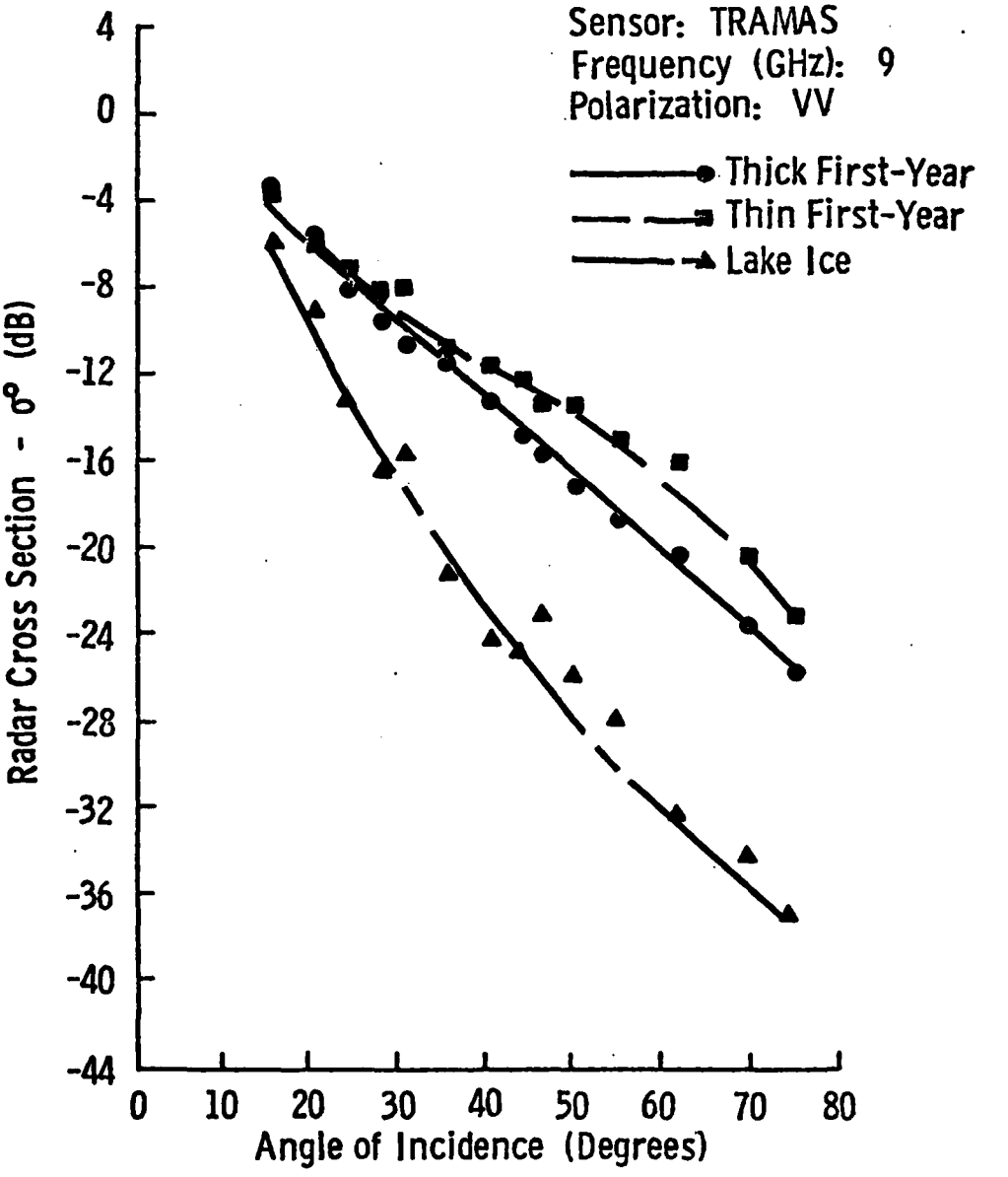

Figure 4.3: Average Scattering Coefficient of Thick First-Year, Thin First-Year, and Lake Ice at 9 GHz (March 1979)

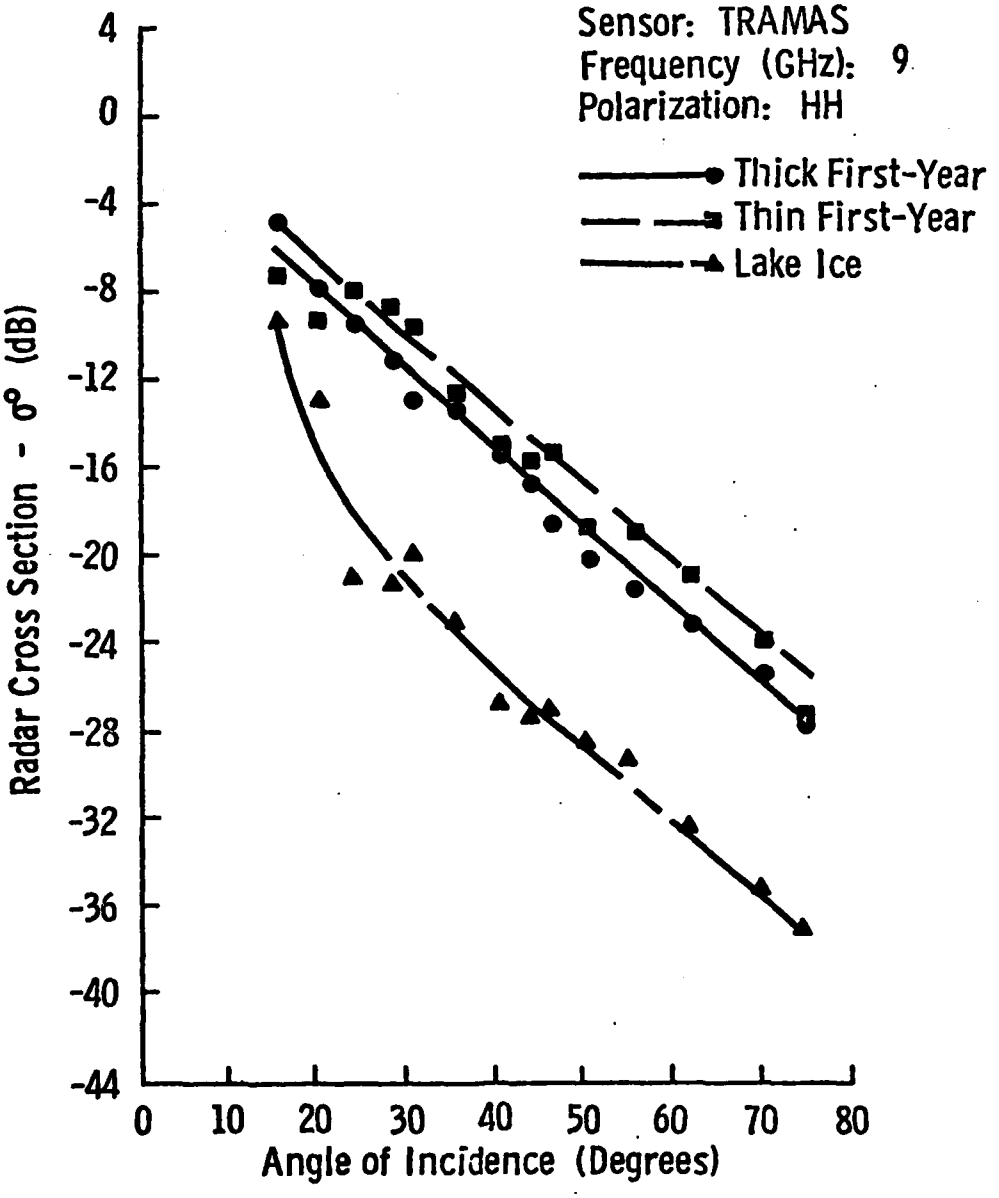

Figure 4.4: Average Scattering Coefficient of Thick First-Year, Thin First-Year, and Lake Ice at 9 GHz (March 1979)

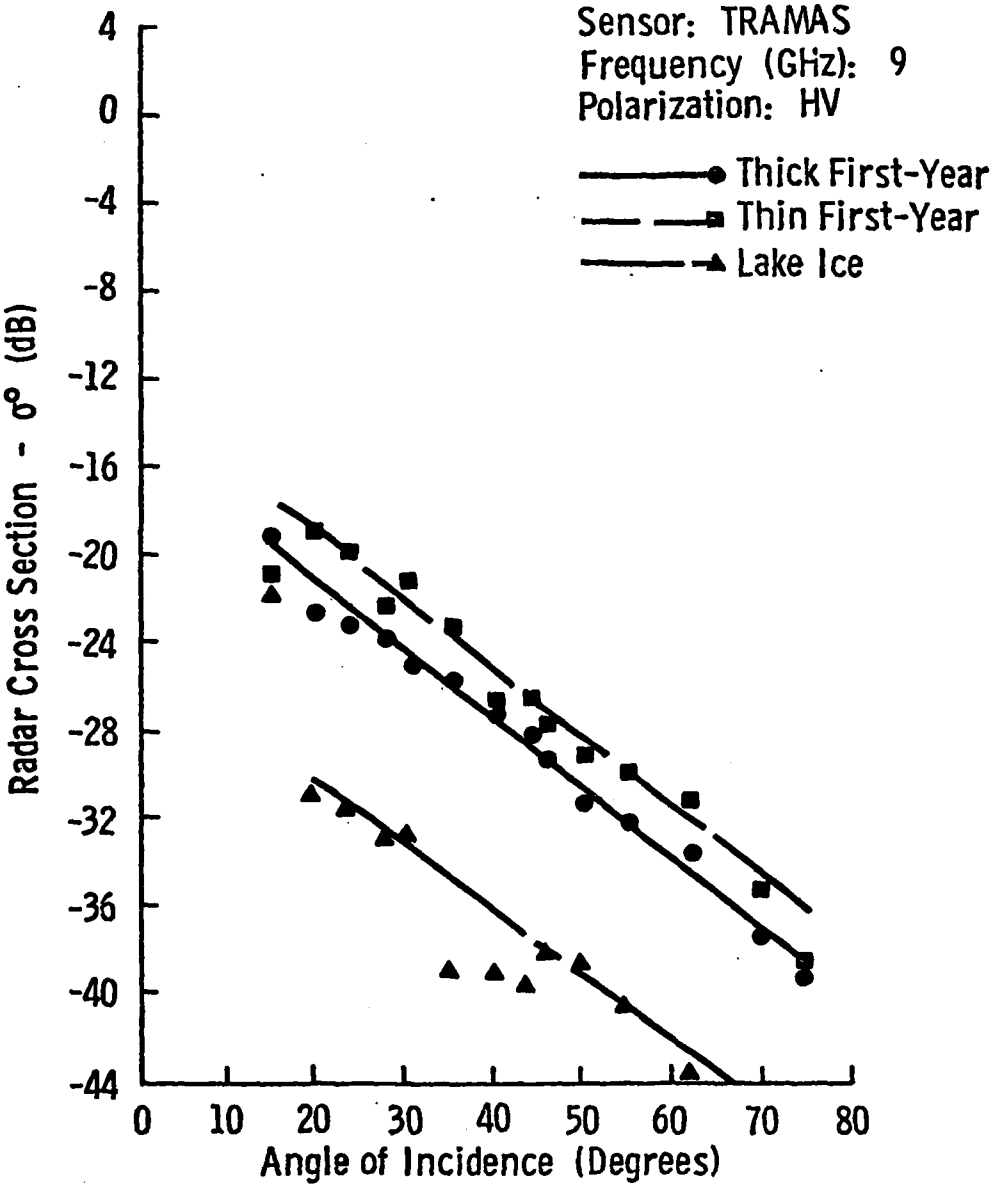

Figure 4.5: Average Scattering Coefficient of Thick First-Year, Thin First-Year, and Lake Ice at 9 GHz (March 1979)

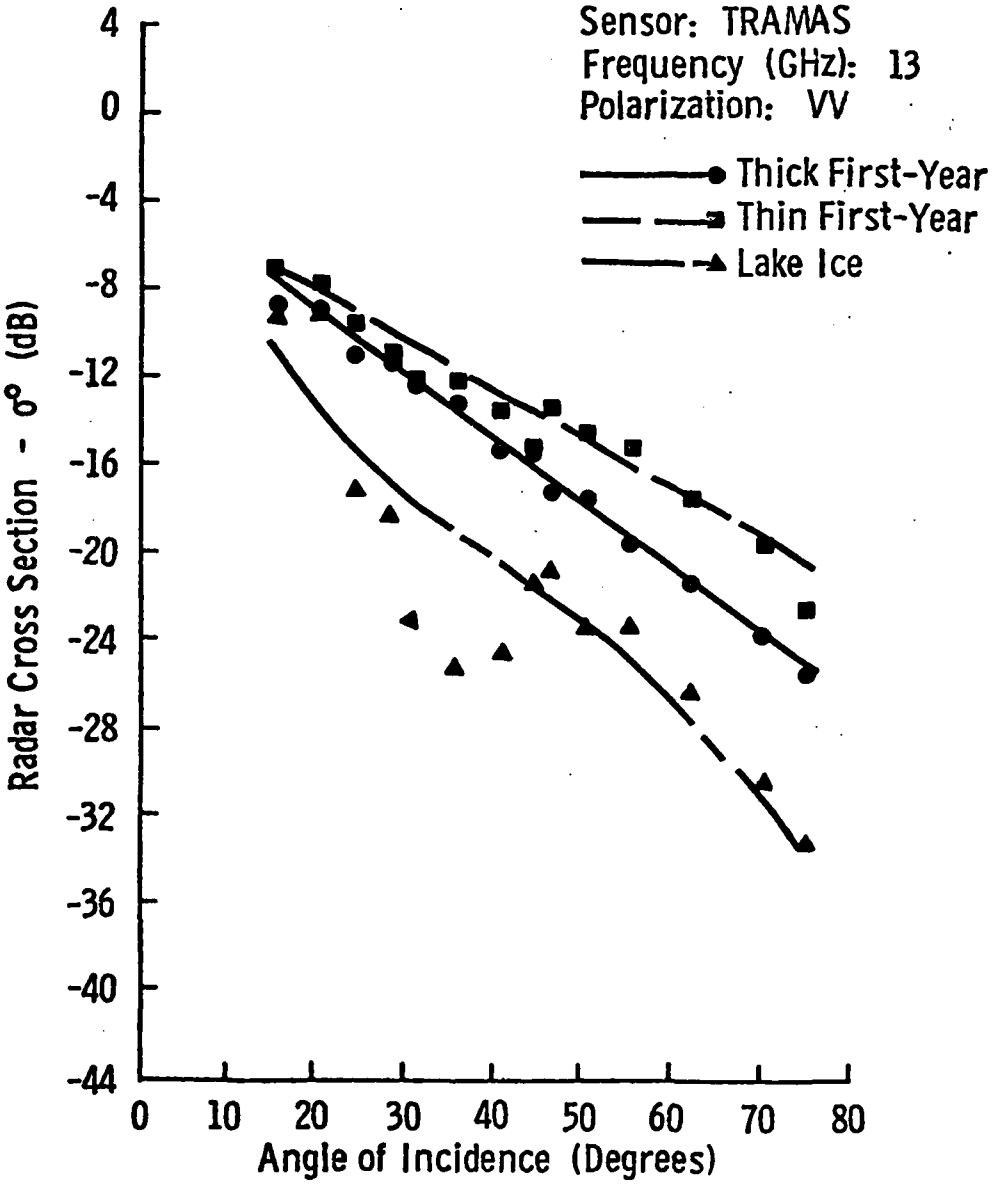

Figure 4.6: Average Scattering Coefficient of Thick First-Year, Thin First-Year, and Lake Ice at 13 GHz (March 1979)

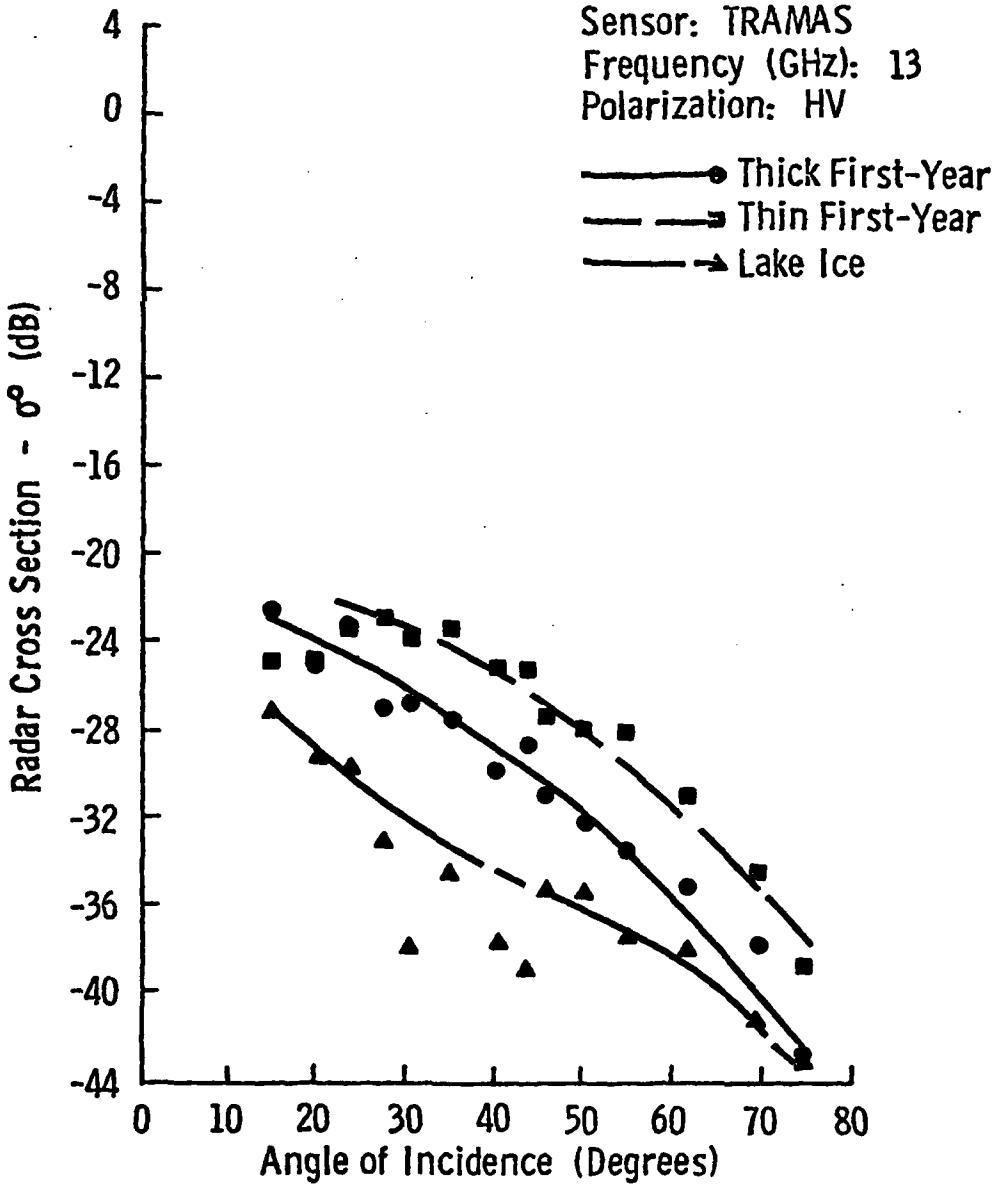

Figure 4.7: Average Scattering Coefficient of Thick First-Year, Thin First-Year, and Lake Ice at 13 GHz (March 1979)

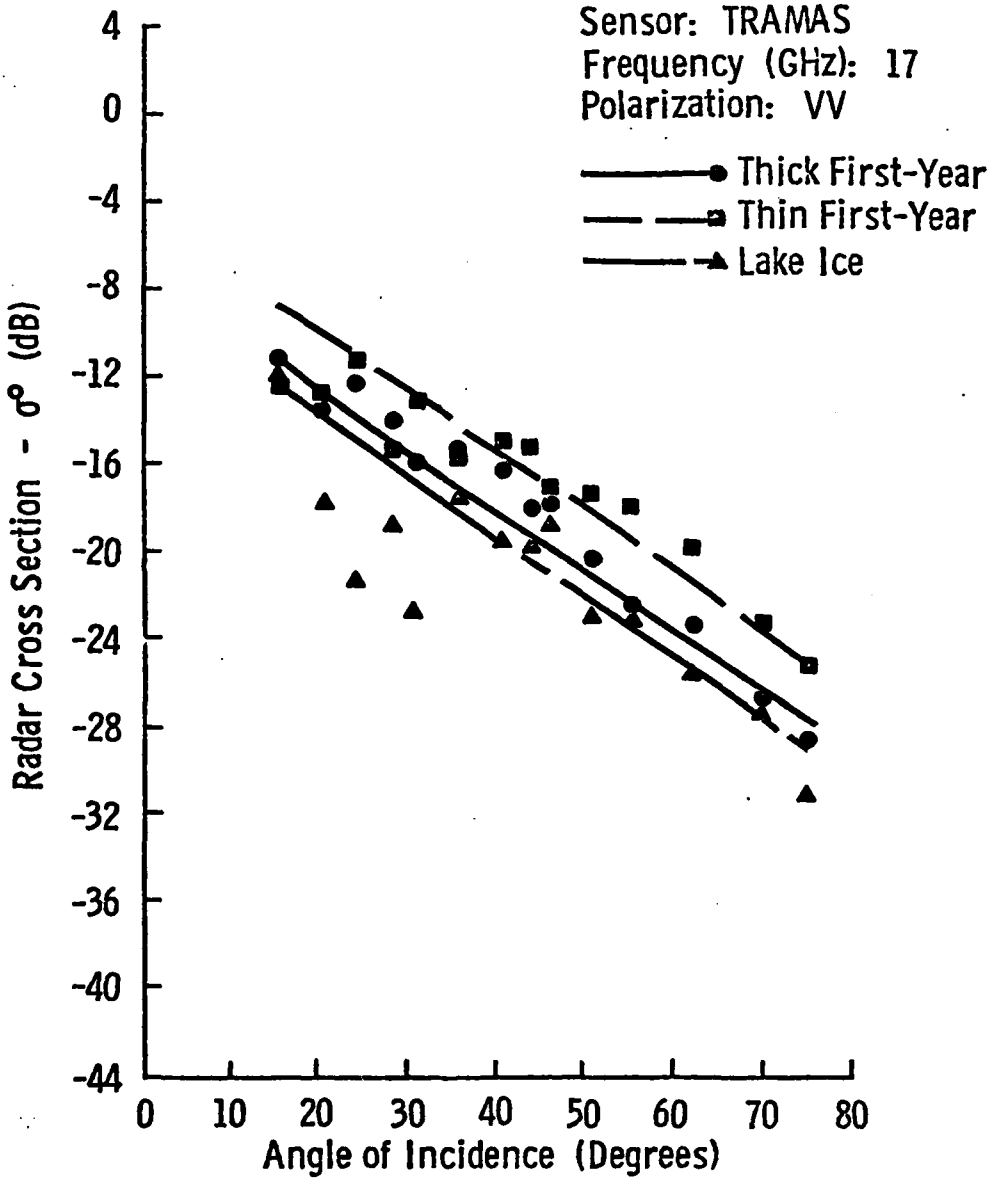

Figure 4.8: Average Scattering Coefficient of Thick First-Year, Thin First-Year, and Lake Ice at 17 GHz (March 1979)

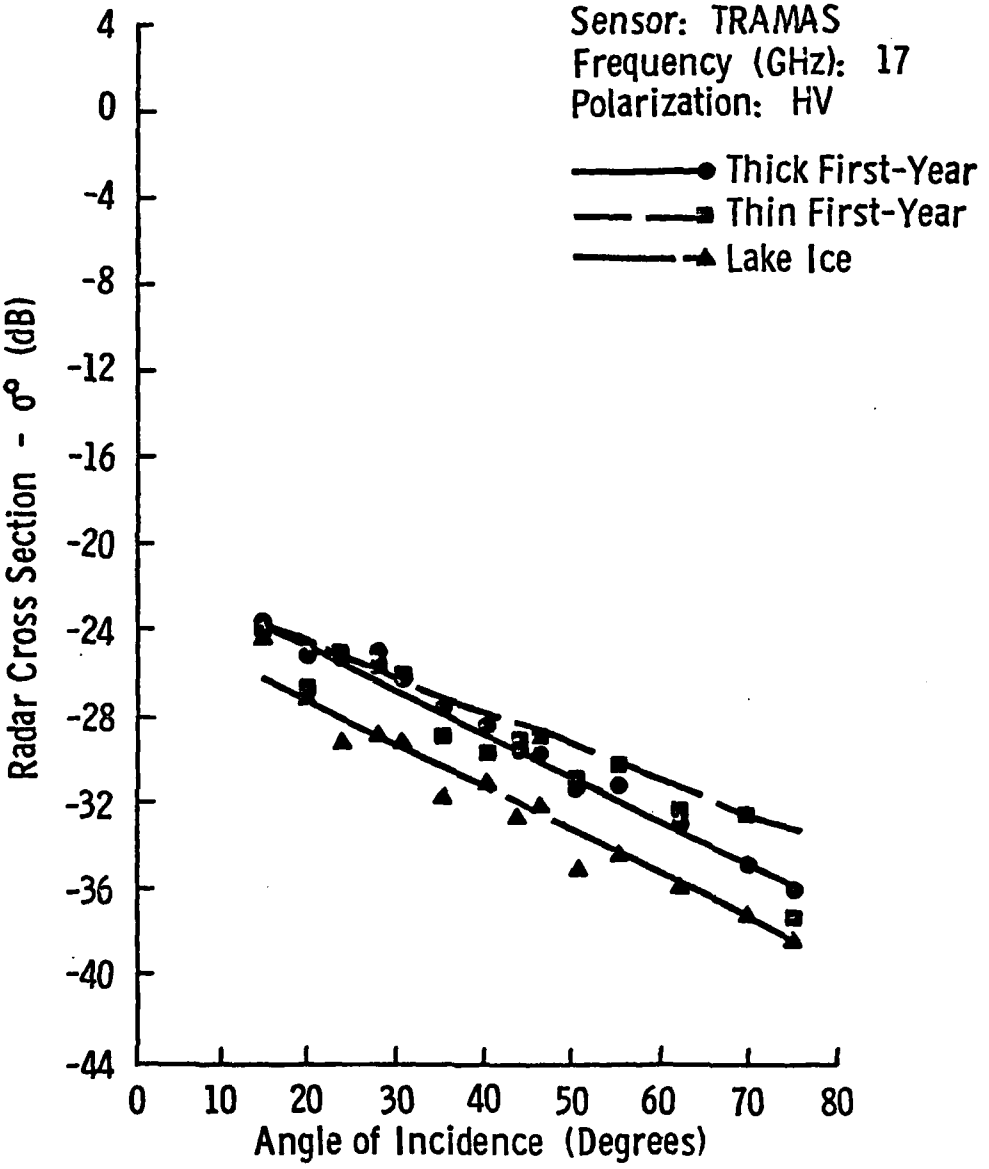

Figure 4.9: Average Scattering Coefficient of Thick First-Year, Thin First-Year, and Lake Ice at 17 GHz (March 1979)

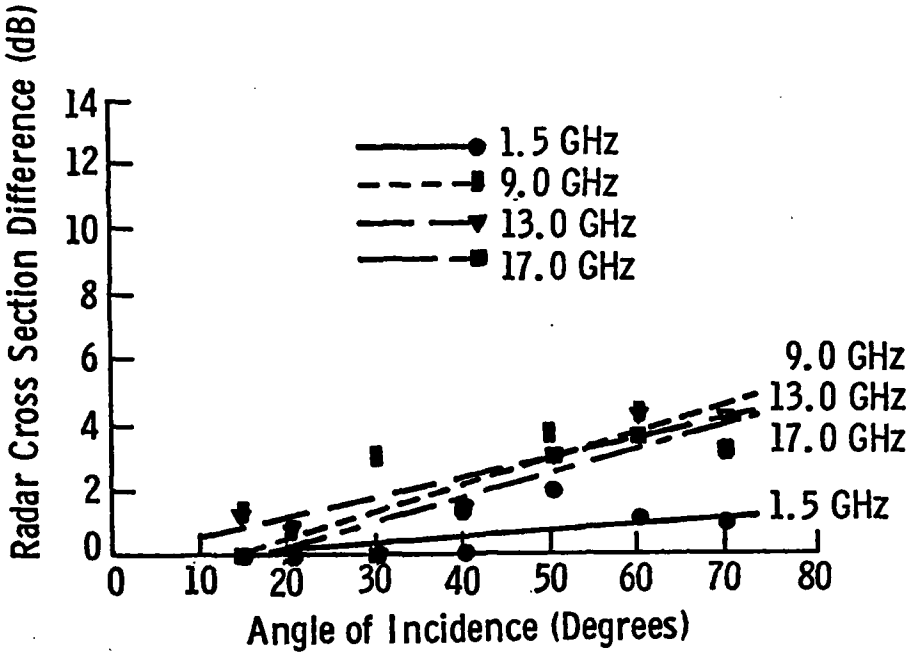

Figure 4.10: Difference Between Radar Cross-Section of Thin First-Year and Thick First-Year Sea Ice at 1.5, 9.0, 13.0, and 17.0 GHz with Vertical Polarization (TRAMAS, March 1979)

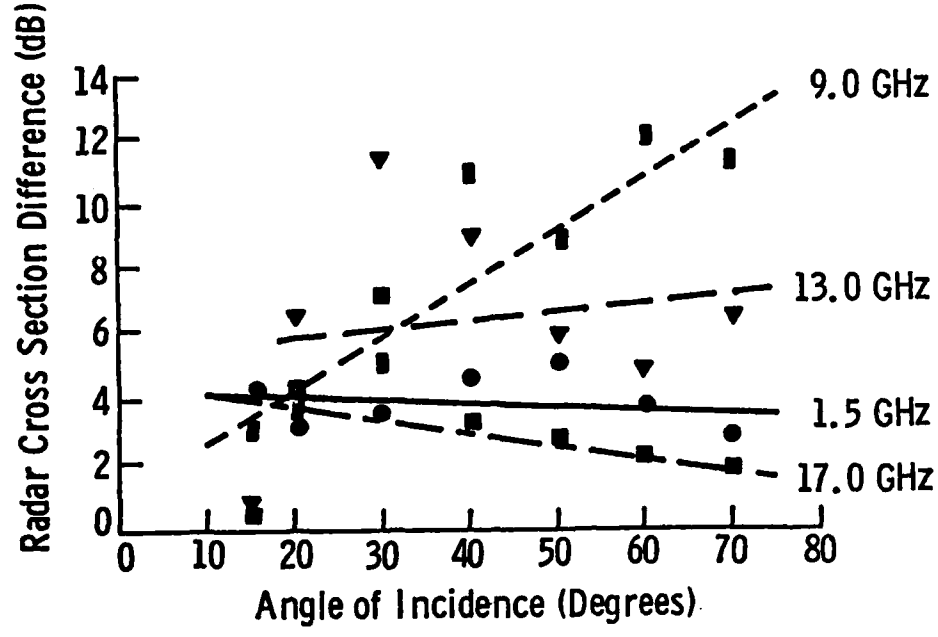

Figure 4.11: Difference Between Radar Cross-Section of Thick First-Year Sea Ice and Lake Ice at 1.5, 9.0, 13.0, and 17.0 GHz with Vertical Polarization (TRAMAS, March 1979)

for all ice types occurs for a frequency of 9 GHz, vertical polarization, and incidence angles greater than 40°.

Notice should also be taken of the correlation between the salinity of the ice type and the magnitude of the scattering coefficients for each type. Thin first-year sea ice, which has the highest salinity, also produced the highest scattering coefficient. Lake ice, which has a very low salinity, produced the lowest scattering coefficient. Thick first-year sea ice which has a salinity that is lower than that of thin first-year sea ice also had scattering coefficients which were lower than those for the thin ice but higher than the lake ice. This observation is also true for the HELOSCAT data to be discussed in the next section.

An investigation of the effects of snow cover on the backscatter from lake ice was performed as a part of this experiment. The results of this investigation at 9 (VV and HH) and 17 (VV and HH) GHz are shown in Figures 4.12 through 4.15. Initial measurements were made without the snow cover being disturbed by the experimenters. Old snowmobile tracks and small surface features caused by the wind were characteristic of this hard-packed snow cover. This surface is labeled "normal" on the graphs. In contrast to the normal surface, a "rough" surface was created by driving a snowmobile across the target area several times. This resulted in loosening the snow pack and produced an uneven distribution of snow cover. Next a "very rough" surface condition was created by making a grid of grooves in the snow cover. The grooves were approximately 4 cm deep and 3 cm wide, spaced 15 cm apart. The final step of the experiment was the complete removal of the snow cover from the target area.

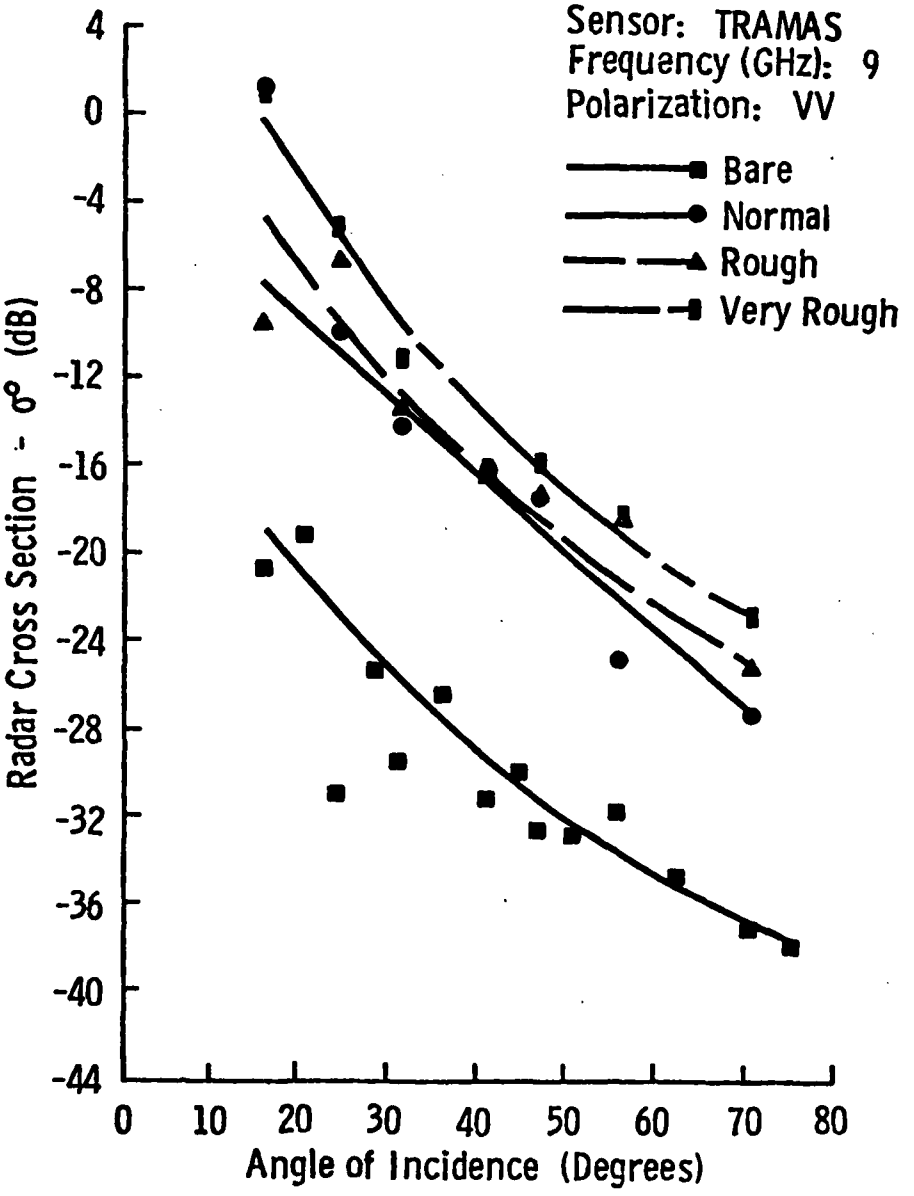

Figure 4.12: Scattering Coefficient of Lake Ice with Bare, Normal, Rough, and Very Rough Snow Cover Conditions at 9 GHz (March 1979)

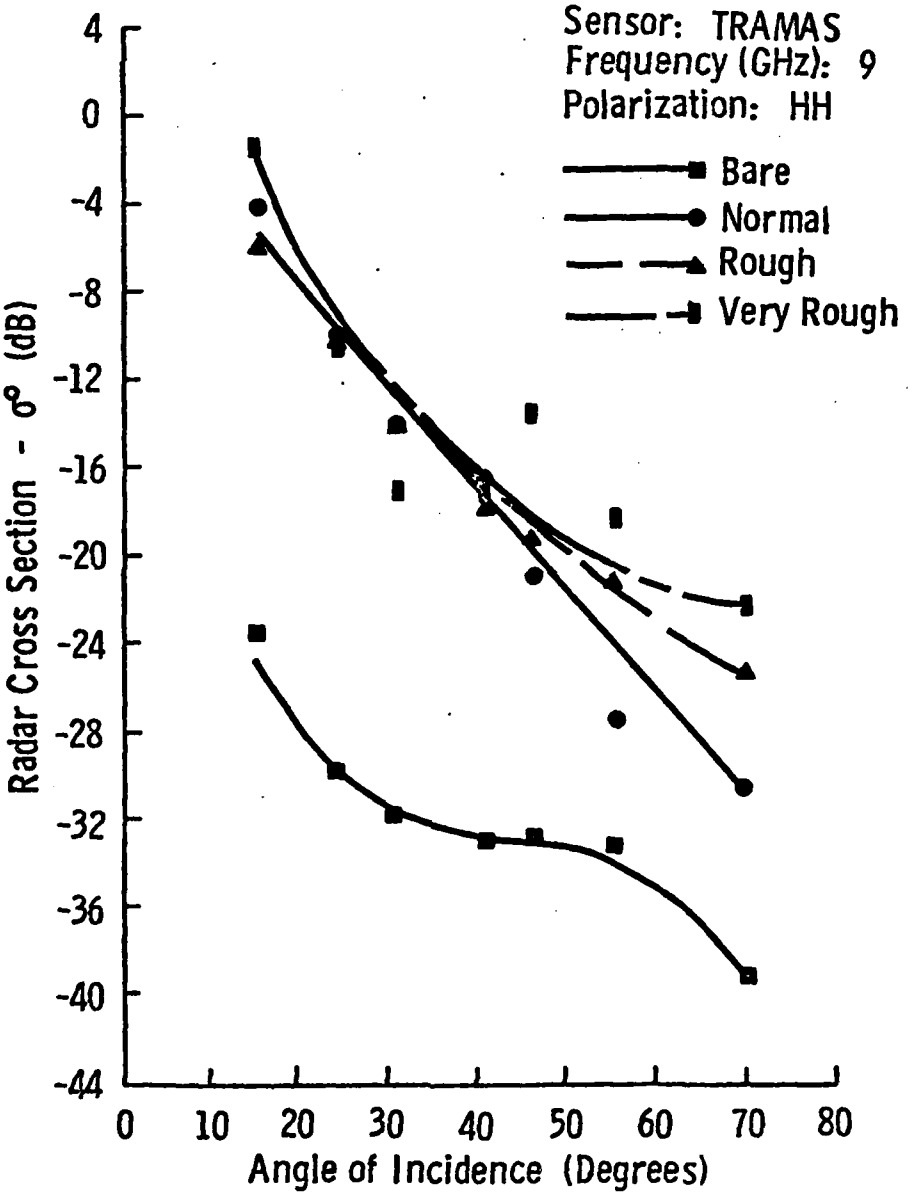

Figure 4.13: Scattering Coefficient of Lake Ice with Bare, Normal, Rough, and Very Rough Snow Cover Conditions at 9 GHz (March 1979)

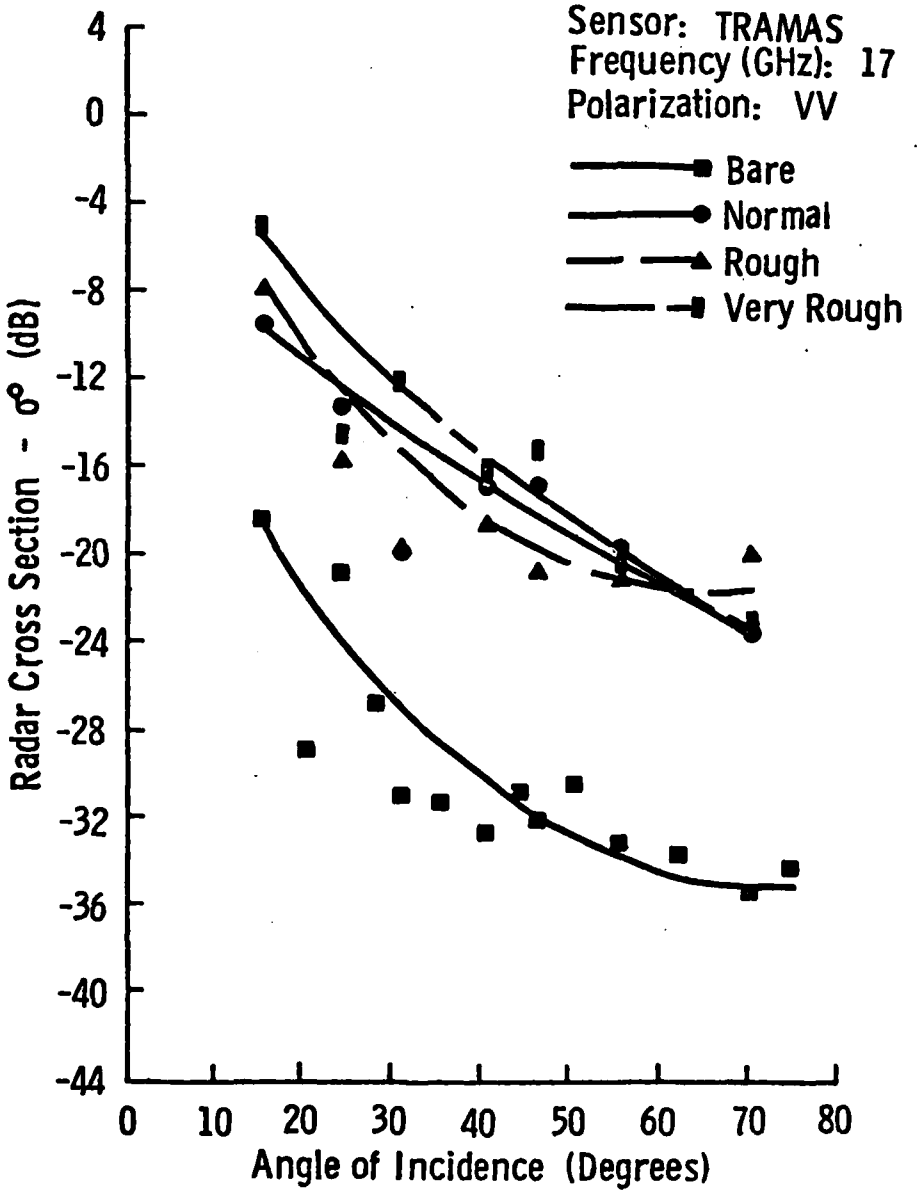

Figure 4.14: Scattering Coefficient of Lake Ice with Bare, Normal, Rough, and Very Rough Snow Cover Conditions at 17 GHz (March 1979)

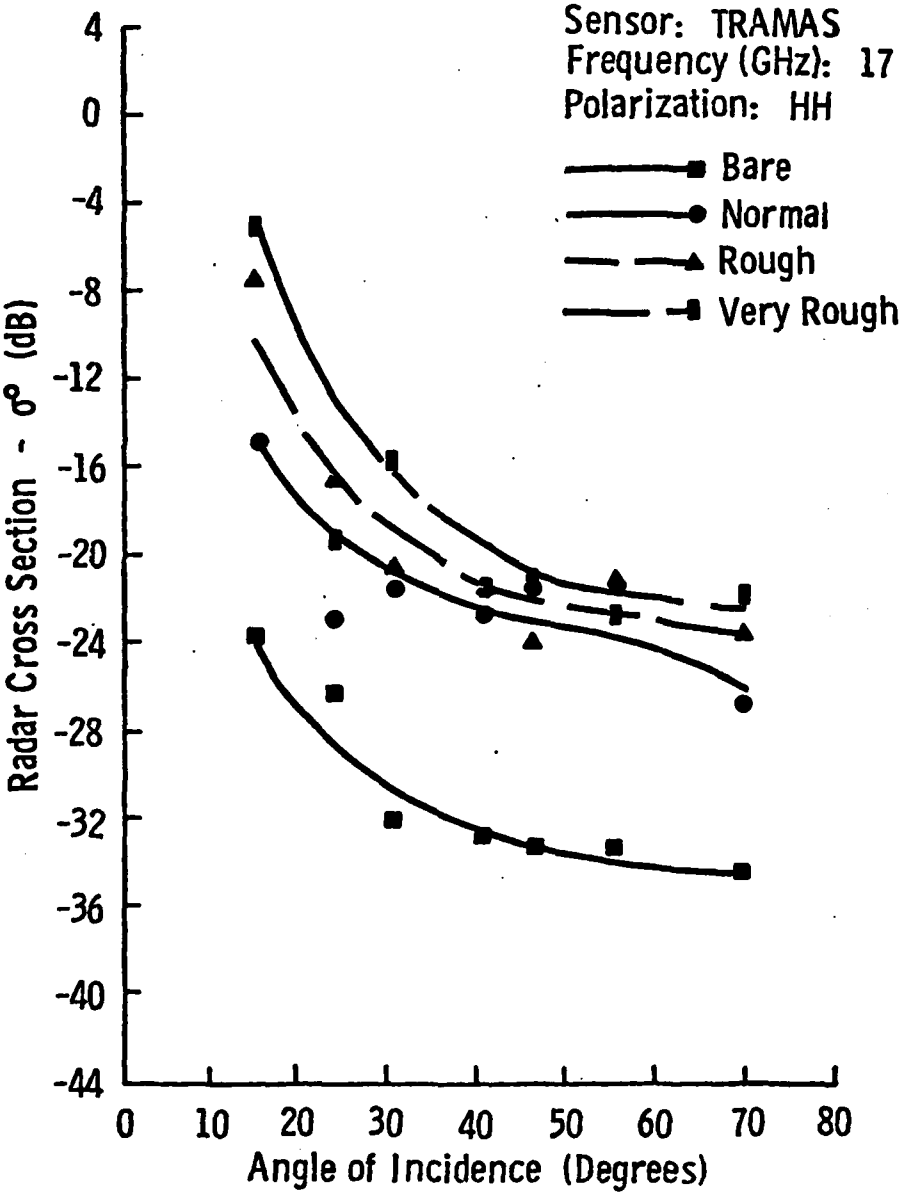

Figure 4.15: Scattering Coefficient of Lake Ice with Bare, Normal, Rough, and Very Rough Snow Cover Conditions at 17 GHz (March 1979)

As is indicated by Figures 4.12 through 4.15, the horizontally polarized scatter is affected to a greater extent by the roughening of the snow surface than the vertically polarized scatter. It is apparent that the radar signal is affected by the orientation of the edges of the air/snow interfaces created by the roughened surface and that the orientation of the grooves with the horizontal component of the radar signal combined to produce a dominant backscatter characteristic. This is most noticeable for large angles of incidence at the lower frequencies. The vertically polarized scatter responses are very similar for the normal and rough cases at all frequencies.

In all cases the scattering coefficient responses for the bare-surface lake were dramatically lower than the snow-covered lake ice responses. The difference averaged 8 dB or greater. Similar results during the April 1978 experiment at Point Barrow, Alaska for snow cover on an undeformed area of thick first-year sea ice led the experiment group to expect such a response for lake ice but not the large differences that were observed. Clearly it is apparent that snow cover is a large contributor to the backscatter from lake ice. Thus, even at these very cold temperatures, the effect of snow cover must be taken into account when extracting information from imagery of frozen lakes. It is also necessary to be aware of the snow surface roughness since it has a measurable effect on backscatter return, especially for the lower X-band frequencies, horizontal polarization, and large incidence angles.

4.3 Ku-X-Band HELOSCAT Results

Angular responses of scattering coefficients obtained with the HELOSCAT system for 9, 13, and 17 GHz and vertical polarization are

shown in Figures 4.16, 4.17, and 4.18. Thick first-year sea ice, thin first-year sea ice, brackish sea ice, and fresh-water lake ice were investigated during this phase of the experiment. As observed with the TRAMAS system, these responses are also ordered with respect to salinity. The high salinity ice produces the largest scattering coefficient while the low salinity lake ice produces the lowest scattering coefficients. This trend leads one to expect that brackish ice, which is a combination of river water and sea water, would have a response that is very similar to or slightly lower than the response for thick first-year sea ice. This conclusion is observed to be true for all frequencies.

Results again indicate that discrimination ability is available given the proper selection of incidence angle. This ability is shown in Figures 4.19 and 4.20 where differences in σ^{o} of thick first-year sea ice, thin first-year sea ice, and lake ice at vertical polarization are plotted as functions of frequency and angle of incidence. The separation between thick and thin first-year sea ice is most prominent for the 9 GHz frequency and discrimination capability appears to be good for all angles of incidence between 10° and 70°. The range of separation in this case (2-6 dB) is larger than that observed with the TRAMAS system. There are several factors which may be responsible for this difference. The measurements made with the HELOSCAT system occurred a week later than those of the TRAMAS system and the temperatures were a few degrees higher at that time. Also the area observed with the HELOSCAT system was not exactly the same as the area observed with the TRAMAS system, although it was on the same floe of thick first-year sea ice. It has been observed that returns from different

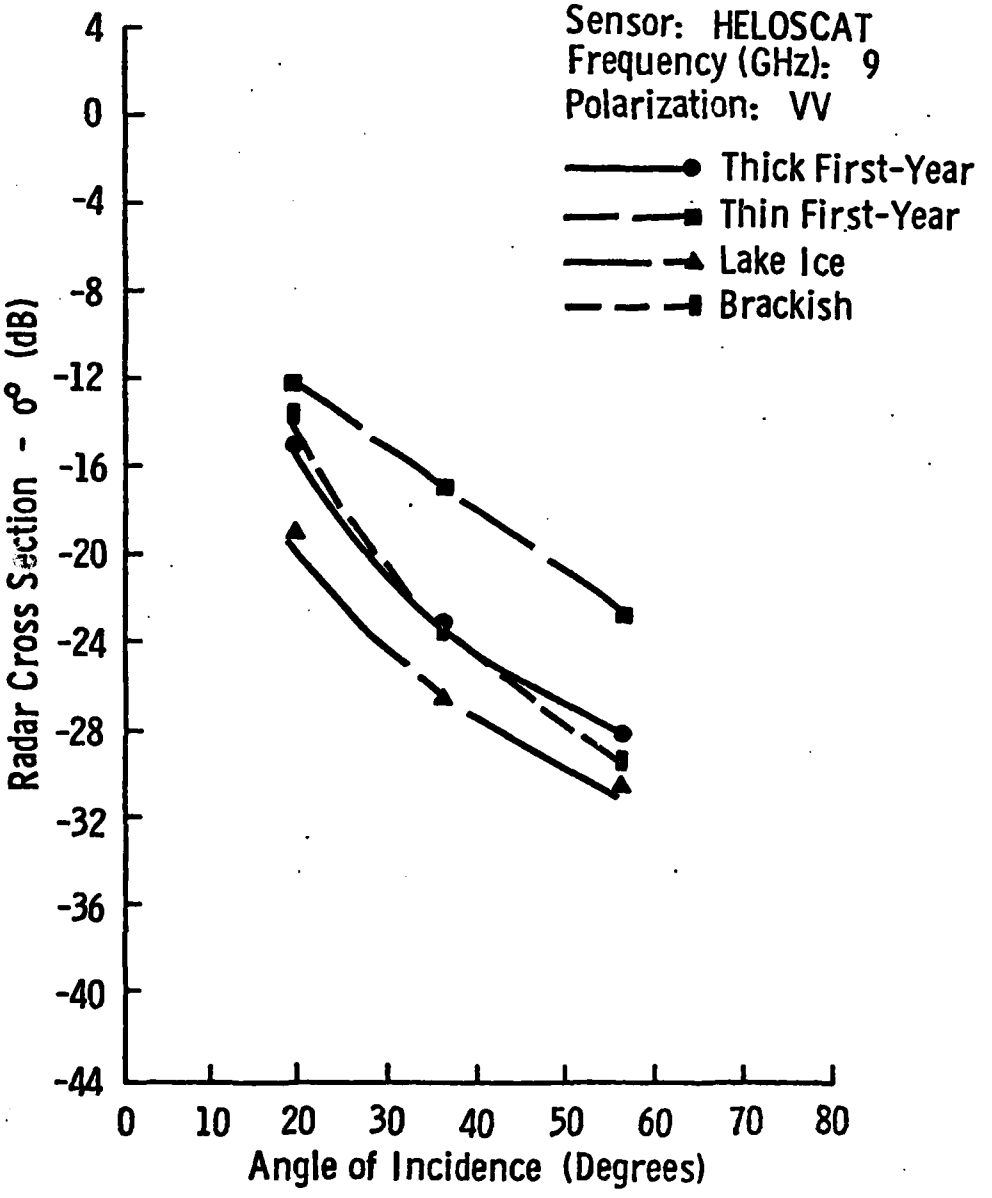

Figure 4.16: Average Scattering Coefficient of Thick First-Year, Thin First-Year, Brackish, and Lake Ice at 9 GHz (March 1979)

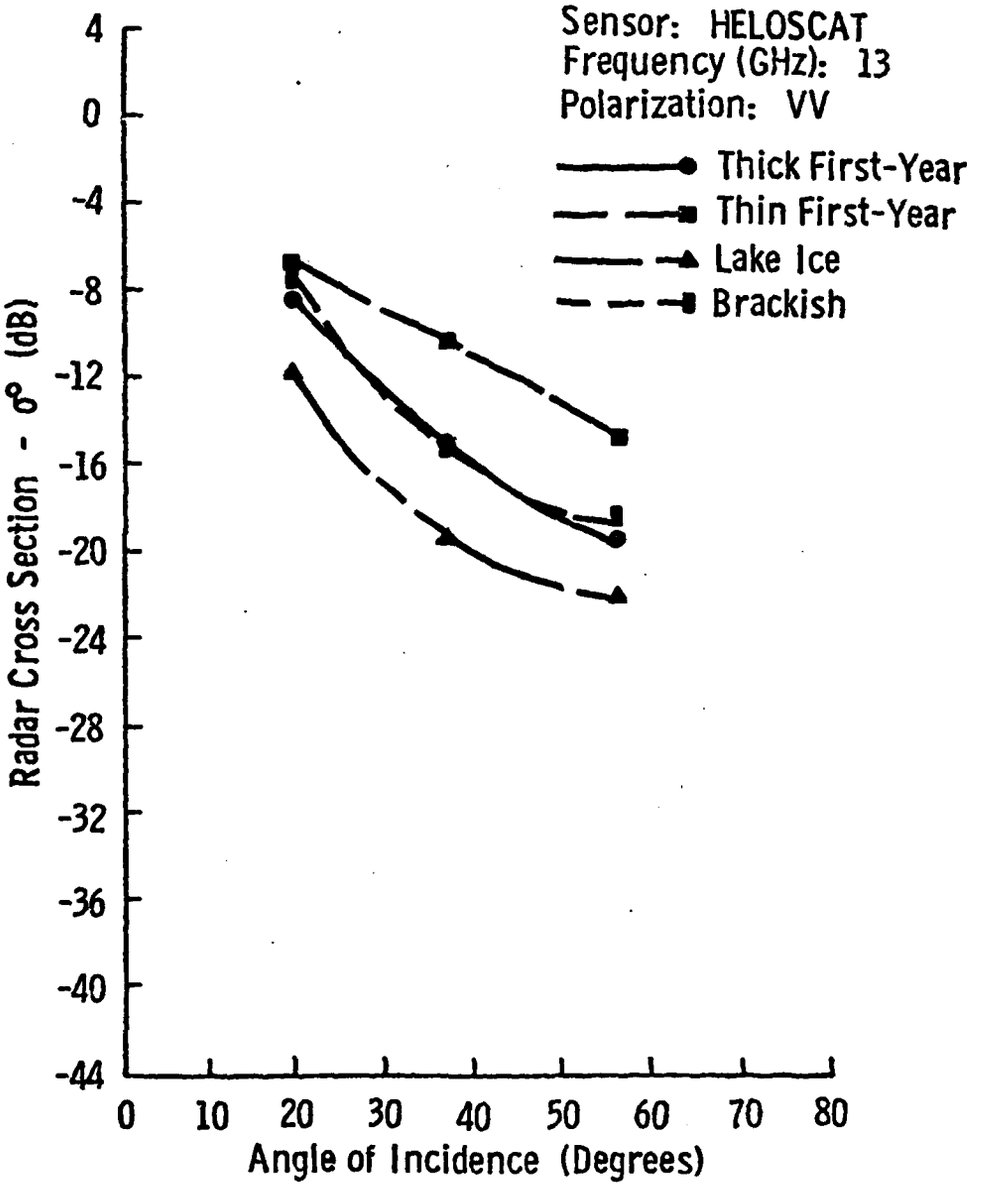

Figure 4.17: Average Scattering Coefficient of Thick First-Year, Thin First-Year, Brackish, and Lake Ice at 13 GHz (March 1979)

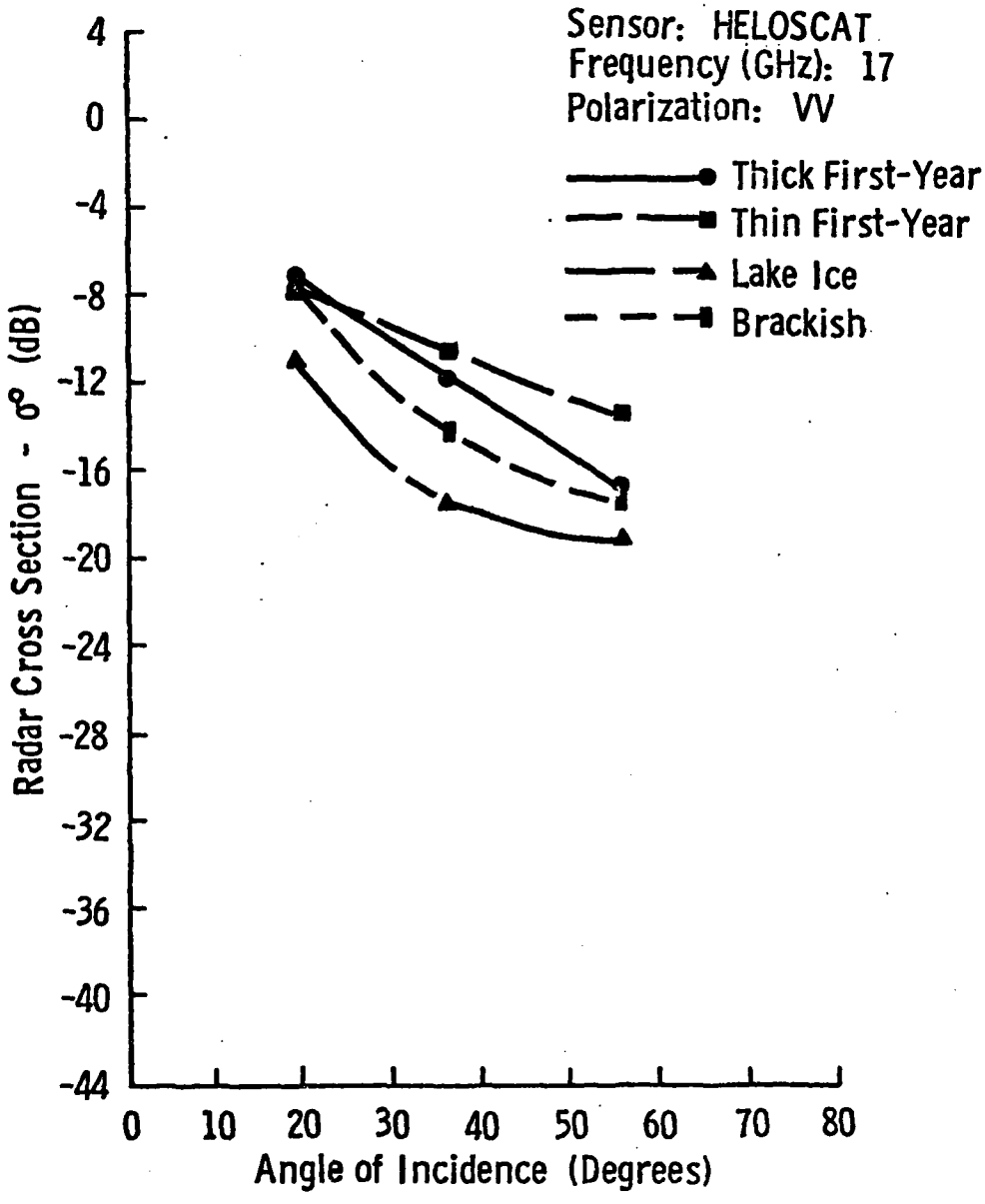

Figure 4.18: Average Scattering Coefficient of Thick First-Year, Thin First-Year, Brackish, and Lake Ice at 17 GHz (March 1979)

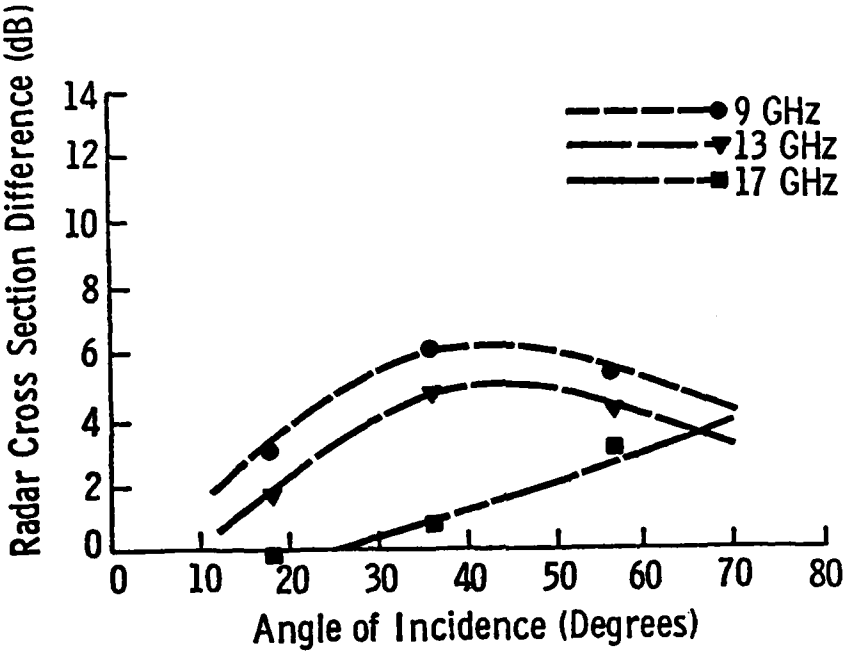

Figure 4.19: Difference Between Radar Cross-Section of Thin First-Year and Thick First-Year Sea Ice at 9.0, 13.0, and 17.0 GHz with Vertical Polarization (HELOSCAT, March 1979)

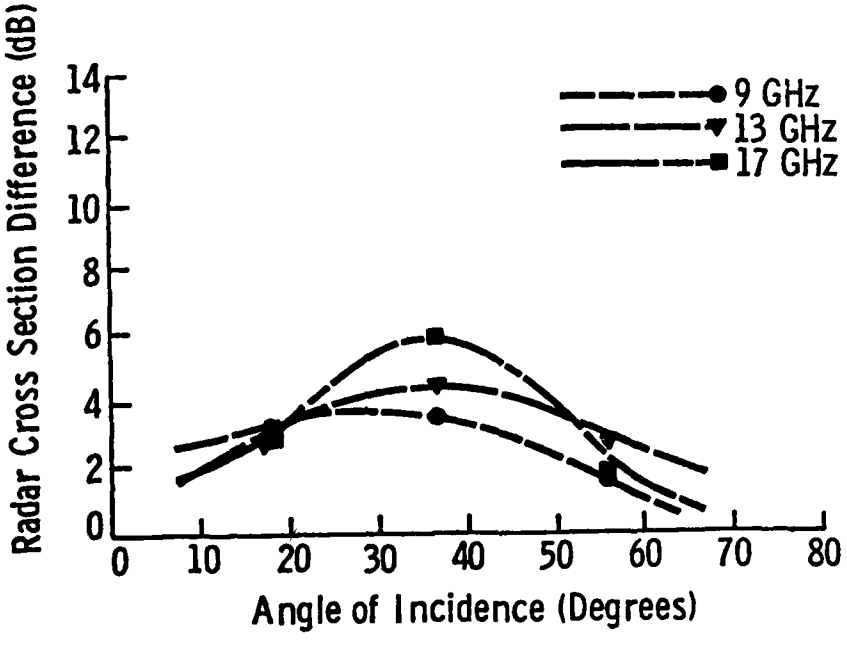

Figure 4.20: Difference Between Radar Cross-Section of Thick First-Year and Lake Ice at 9.0, 13.0, and 17.0 GHz with Vertical Polarization (HELOSCAT, March 1979)

areas of the same floe of ice can vary by as much as 2-3 dB. Finally, the thin first-year sea ice was located in the shear zone. The dynamic nature of this area can be responsible for significant changes in the physical properties of the ice in very short time periods. Discrimination of thick first-year sea ice from lake ice appears to be possible for incident angles between 20° and 60°. The greatest difference occurs at 40° for 17 GHz.

4.4 Comparison of TRAMAS and HELOSCAT Results

During the analysis of the 1978 data from Point Barrow, Alaska, it was observed that the angular responses of the radar cross-section at 8-18 GHz frequencies could be reasonably fit with a straight line for angles of incidence between 10° and 70°. The straight lines were obtained by linear regression using the average (a magnitude average expressed in dB) scatter obtained from multiple looks at a given site. This observation was also found to be true for the 1979 Tuktoyaktuk data. For a 1 percent confidence, the correlation coefficient for the measurements needs to be greater than .89. Some of the regressions of the 1979 data are borderline by this criterion, but the majority have correlation coefficients of .97 or better, which indicates that straight lines are a reasonable fit for these angular responses.

Comparison of the regression lines of the TRAMAS and HELOSCAT data provide a quick indication of similarities between the two data sets. Slopes and 40° intercepts of the regression lines for thick first-year, thin first-year, brackish, and lake ice at 9, 13, and 17 GHz frequencies are tabulated in Table 4.1. Except for lake ice at

TABLE 4.1

COMPARISON OF TRAMAS AND HELOSCAT RESULTS

		TRAMAS		HELOSCAT	
	Frequency	Slope	40° Intercept	Slope	40° Intercept
Thick First-Year	9	-.35	-13.20	-.33	-23.07
	13	-.29	-15.15	-.28	-15.25
	17	-.25	-17.18	-.25	-12.83
Thin First-Year	9	-.28	-11.30	-.27	-18.20
	13	-.22	-13.06	-.21	-11.22
	17	-.20	-16.02	-.16	-11.17
Lake	9	-.48	-21.09	-.29	-26.05
	13	-.32	-21.10	-.26	-18.68
	17	-.21	-20.72	-.21	-16.53
Brackish	9			-.40	-23.36
	13			-.29	-14.75
	17			-.24	-13.86

9 GHz the slopes of the angular responses are nearly identical in all cases. This demonstrates that the HELOSCAT system, with only three angles of incidence, has the capability to provide as much angular information as the TRAMAS system with its fourteen incidence angles.

There is a problem, however, as indicated by the 40° intercepts. The 9 GHz intercept for the TRAMAS system is higher than that for the HELOSCAT. At 13 GHz they are nearly identical while at 17 GHz the level of the HELOSCAT intercept is higher. The cause of this inverse trend is recognized by viewing the frequency responses for the two systems shown in Figures 4.21 and 4.22. Thick and thin first-year sea ice have a response which decreases with increasing frequency for the TRAMAS system, but these types have a response which increased for the HELOSCAT system.

Frequency responses for the 1977 and 1978 data sets were found to increase with increasing frequency. Comparison of the lake ice responses of these two years with the lake ice response for 1979 indicates a good deal of similarity. Analysis of Luneberg-lens calibration data for these three experiments also indicates that the frequency responses of the lens return are very similar. This leads to the conclusion that the 1979 TRAMAS data is accurate and that the frequency response for the first-year ice types does indeed decrease with increasing frequency. The fact that the first-year ice studied in 1979 was further offshore than that studied during 1977 and 1978 may be responsible for the difference in frequency responses.

The question is: what causes HELOSCAT data from the same ice sites to have a different frequency response than the TRAMAS data? Regression of the HELOSCAT data versus frequency with the 9, 10, and

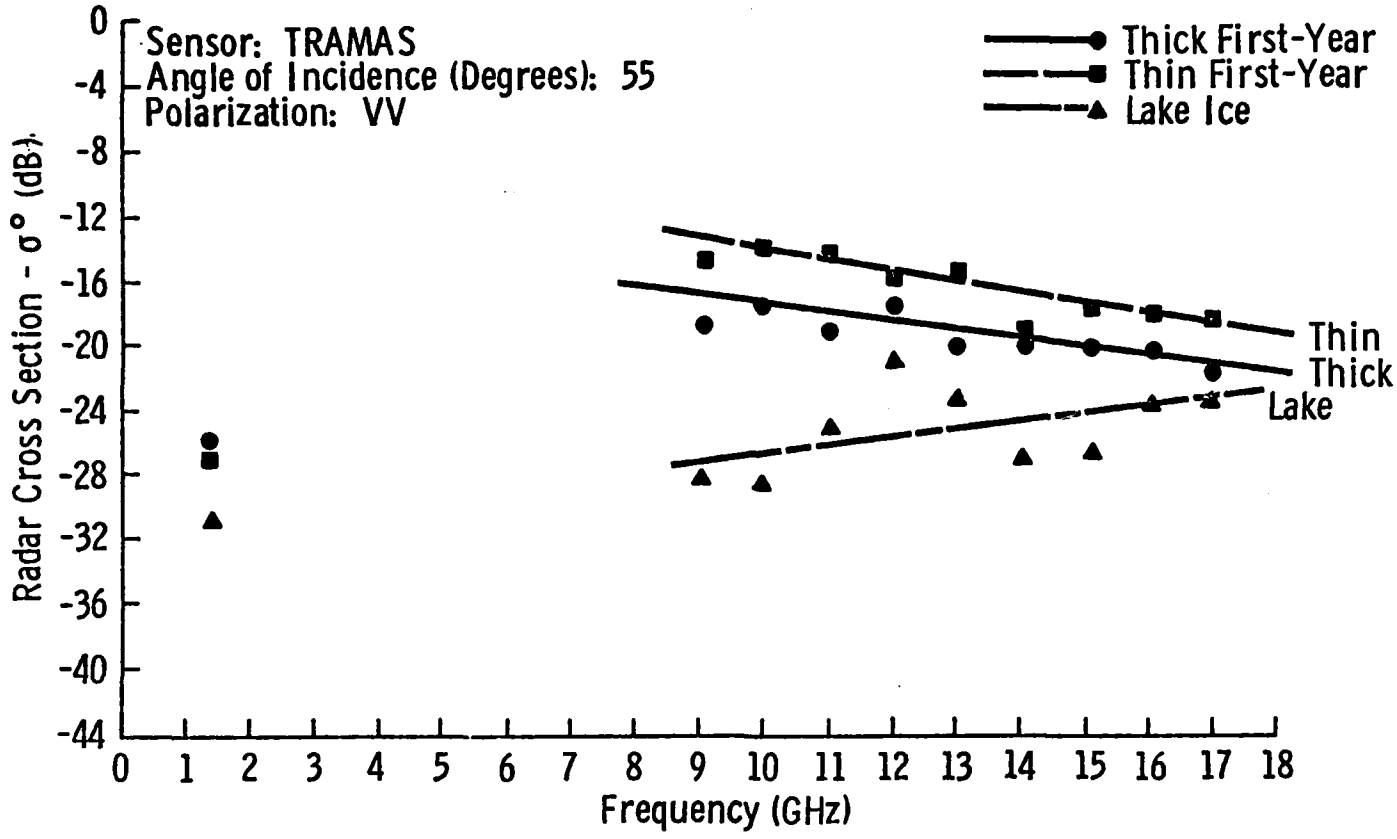

Figure 4.21: Scattering Coefficient Frequency Response of Thick First-Year, Thin First-Year, and Lake Ice (March 1979)

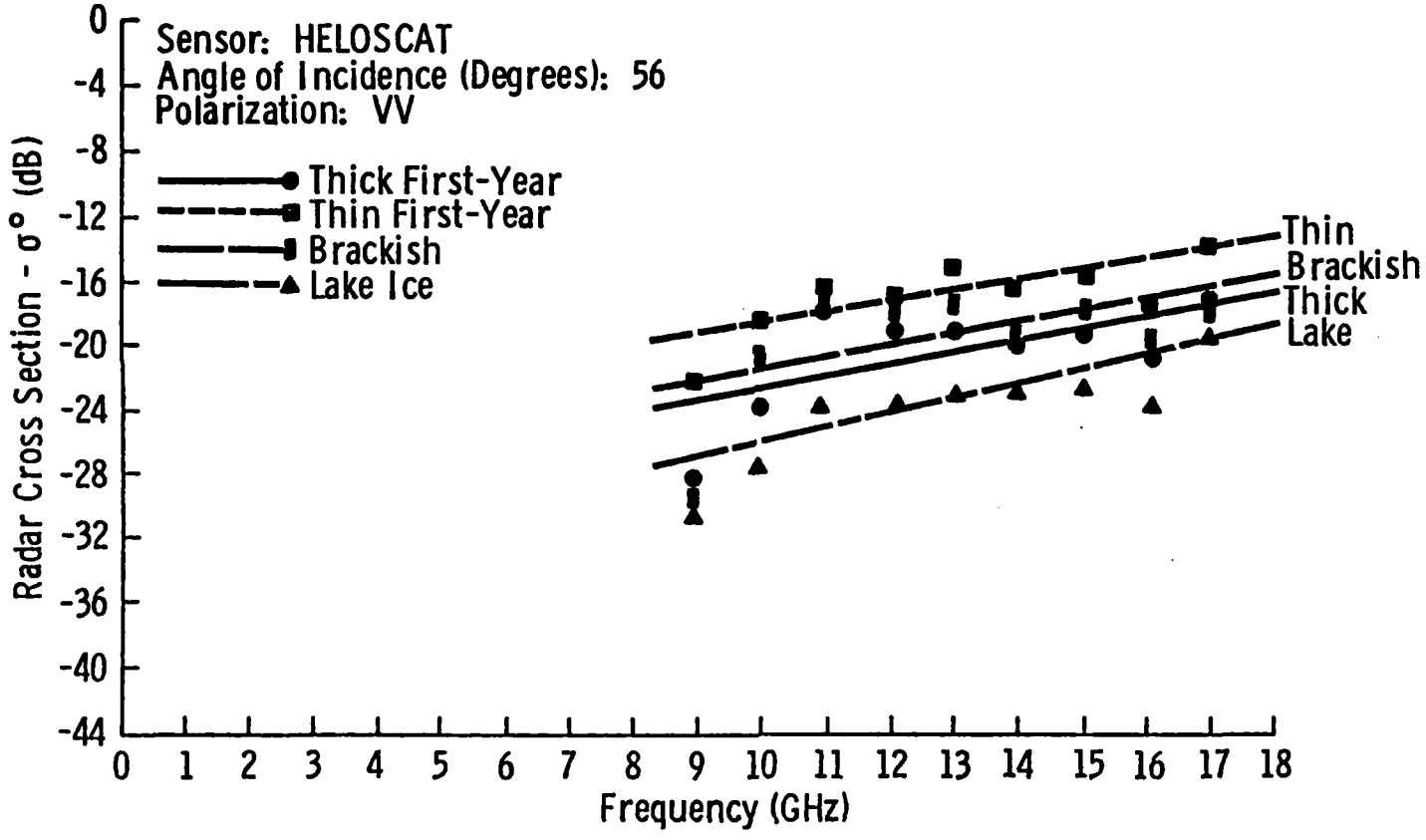

Figure 4.22: Scattering Coefficient Frequency Response of Thick First-Year, Thin First-Year, Brackish, and Lake Ice (March 1979)

17 GHz points neglected results in a trend that looks similar to the trends of the TRAMAS data. The most obvious suspect for this problem is the Luneberg-lens calibration of the HELOSCAT system. The HELOSCAT system is calibrated on the ground with the antennas aimed horizontally at the Luneberg lens reflector which is supported on a stand at some fixed range. There are two potential sources of error in this procedure. The aiming of the antennas and the position of the reflector are very critical. There is also the potential for multi-path ground reflections to affect the measurement. Calculations of this effect indicate that interference magnitudes of greater than 4 dB may be expected. Such interference would produce significant changes in the radar cross-section of the target. Future calibrations of the HELOSCAT system must be conducted in such a manner that this problem is eliminated or corrections established to account for these effects.

5.0 COMPARISON WITH PREVIOUS UNIVERSITY OF KANSAS EXPERIMENTS

Near-surface radar backscatter studies of Arctic sea ice have been carried out on three separate occasions by research teams from the University of Kansas Remote Sensing Laboratory (previous measurements in 1967 and 1970 involved aircraft measurement platforms). These experiments were conducted at Point Barrow, Alaska, during May 1977 and April 1978, and at Tuktoyaktuk, N.W.T., Canada, during March 1979. The ice types investigated during these experiments included multi-year sea ice, thick first-year sea ice, thin first-year sea ice, brackish sea ice, fresh-water inland lake ice, and a small first-year pressure ridge. Studies of thick first-year sea ice and lake ice have occurred in more than one of the experiments and may therefore be compared directly.

The TRAMAS system was used to investigate a fresh-water inland lake which was frozen to the bottom for both the 1977 and 1979 experiments. South Meadow Lake, Site #7 investigated during 1977, was .74 meters in depth and had an 18 cm snow cover. The temperature at the time of this experiment was 2° C. Site T5, investigated in 1979, was a lake 1.8 meters in depth with a 4-8 cm snow cover. Temperature at the time of study was -30° C. Comparisons of angular response for these two sites for VV and HV polarizations at 9 and 17 GHz are presented in Figures 5.1 and 5.2. The response from the lake investigated in 1977 is higher in all cases. The combination of the higher temperature and the heavy snow cover for the 1977 lake are most likely responsible for the observed differences.

Thick first-year sea ice was investigated with the TRAMAS system during all three experiments. Site 3, investigated in 1977, was 1.37

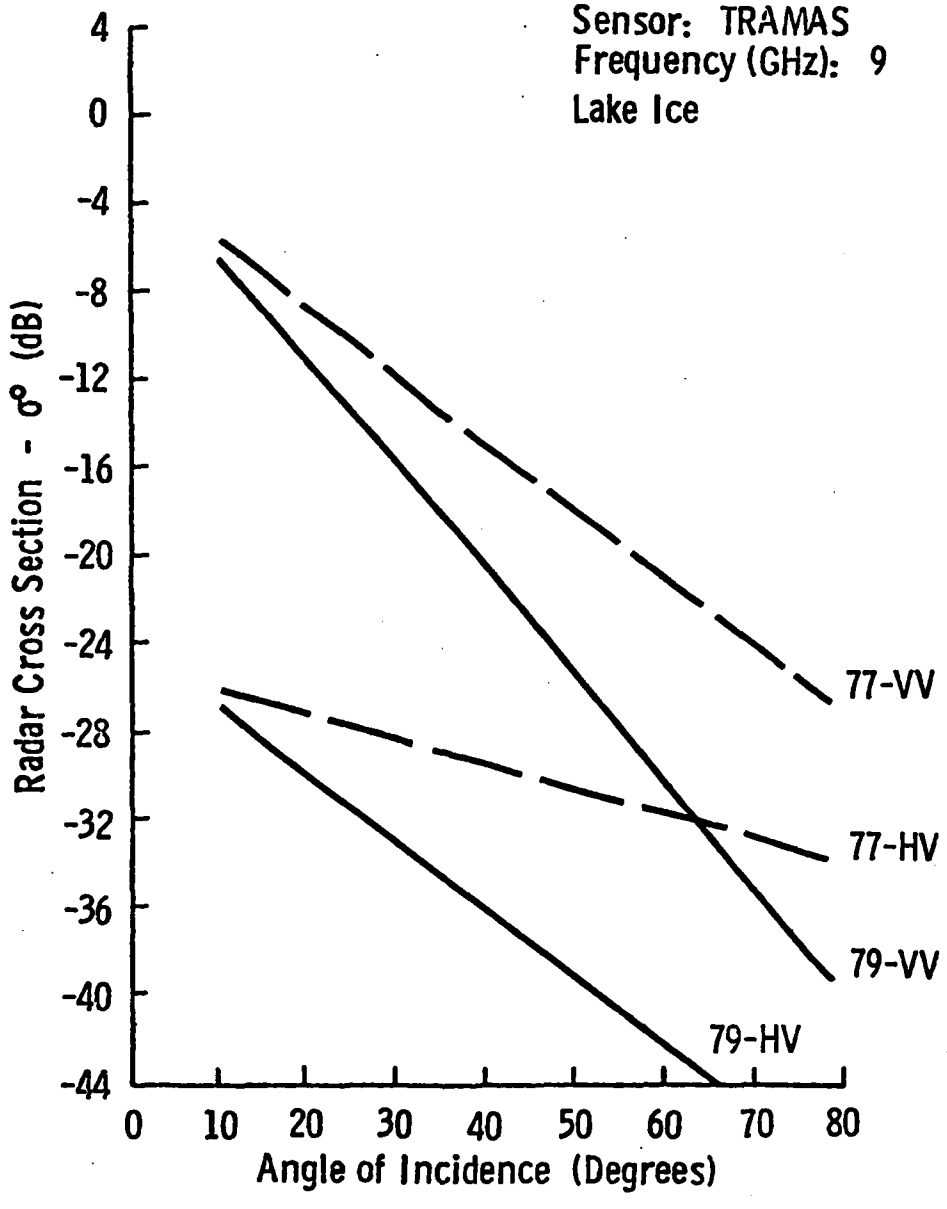

Figure 5.1: Comparison of Radar Cross-Sections of Lake Ice at 9 GHz, Vertical and Cross Polarizations, from the 1977 and 1979 University of Kansas Arctic Experiments

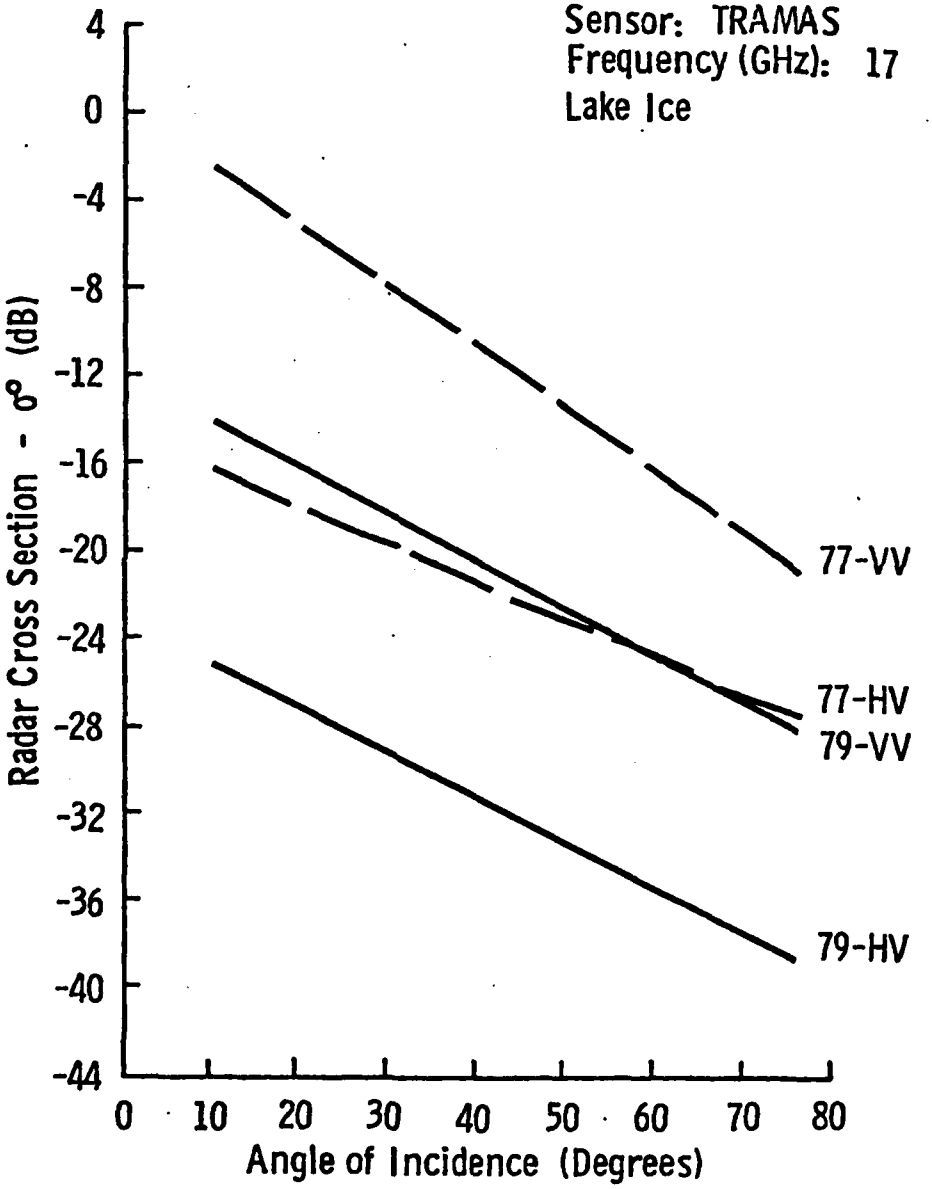

Figure 5.2: Comparison of Radar Cross-Sections of Lake Ice at 17 GHz, Vertical and Cross Polarizations, from the 1977 and 1979 University of Kansas Arctic Experiments

meters thick and had a 2 cm snow cover. The experiment temperature was -10° C. Shorefast thick first-year sea ice was the only type available for study during the TRAMAS portion of the 1978 experiment. The site investigated was 1.68 meters in depth and had a 2 cm snow cover. The average temperature during these experiments was -8° C. Both of the thick first-year sites investigated in 1977 and 1978 were located very close to the shore line. The thick first-year sea ice site, Site A, investigated in 1979 was located approximately 15 miles from the shore. The ice at this site was 1.3 meters thick and had a 1-2 cm snow cover. Experiment temperature was -30° C.

Angular responses for the ice sites with VV and HV polarization at 9 and 17 GHz are shown in Figures 5.3 and 5.4. The responses for 1977 and 1978 at vertical polarization are almost identical for 9 GHz but spread apart as the frequency increases. The 1979 data responses are higher at 9 GHz and then are lower at 17 GHz. This is the decreasing frequency response trend discussed in Section 4.4. The 1979 data also demonstrates a greater separation at all frequencies. These trends may be due to the fact that the 1979 thick first-year sea ice site was further from shore than the preceeding two years' sites or to differences in temperature. Radar imagery has shown that there is a difference between returns from first-year ice located in the shorefast zone and that located in the pack ice region.

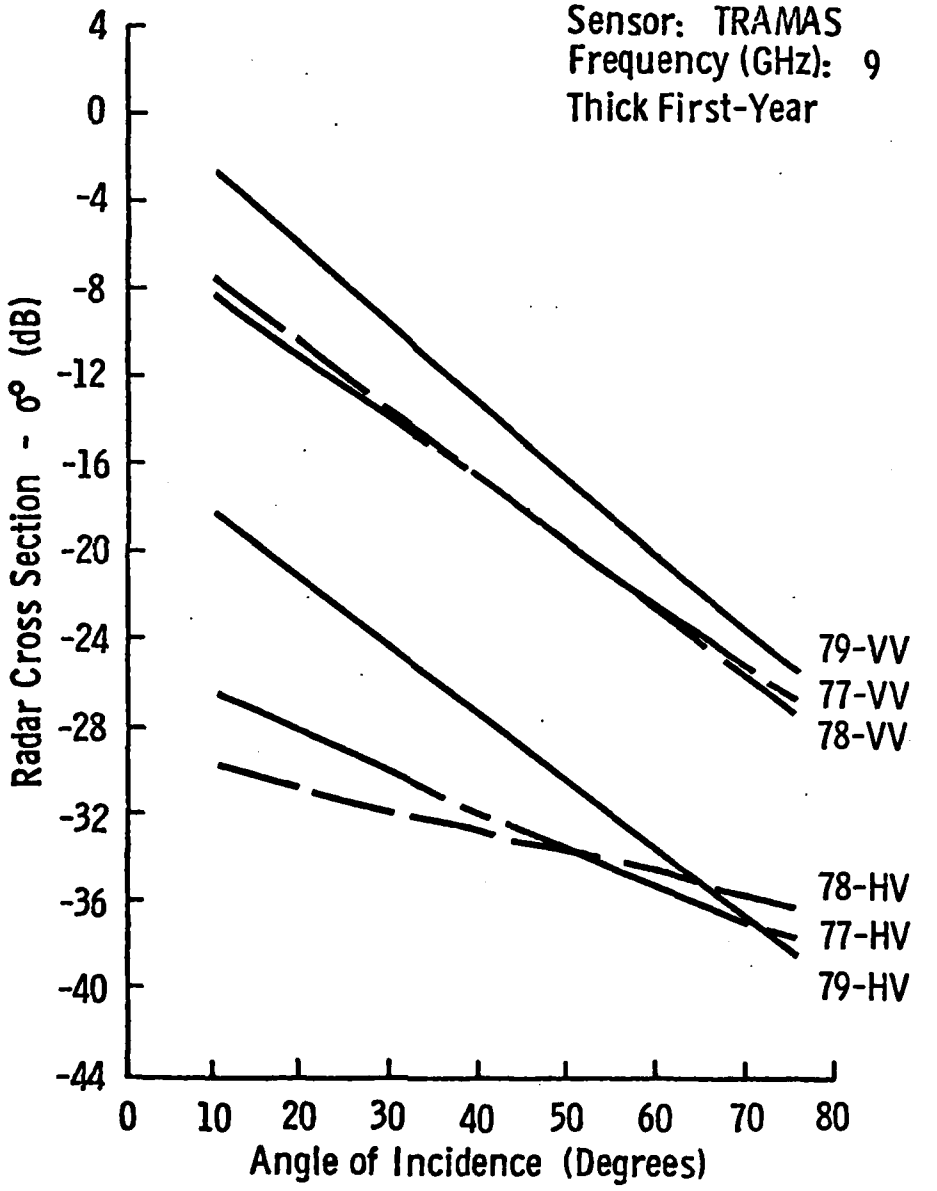

Figure 5.3: Comparison of Radar Cross-Sections of Thick First-Year Sea Ice at 9 GHz, Vertical and Cross Polarizations, from the 1977, 1978, and 1979 University of Kansas Arctic Experiments.

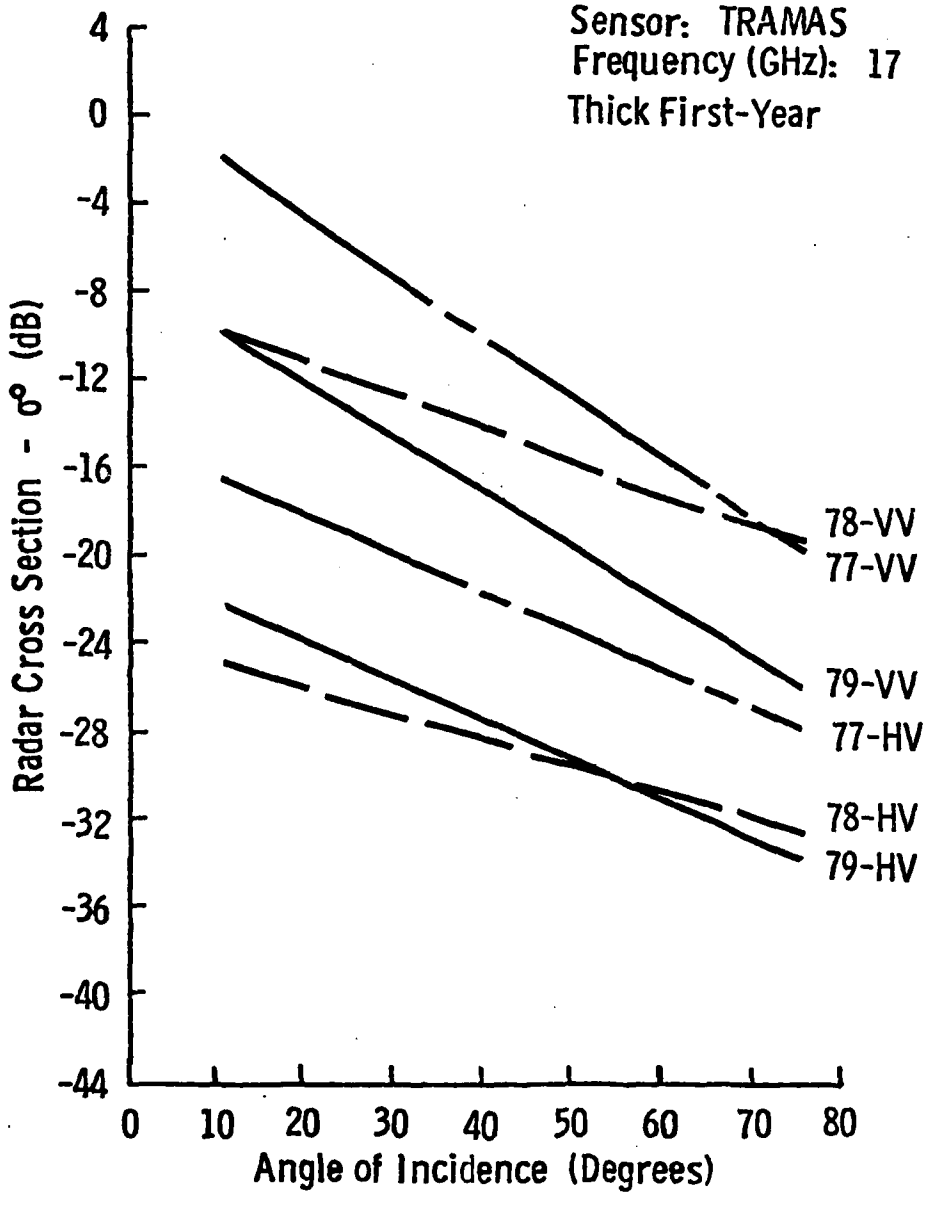

Figure 5.4: Comparison of Radar Cross-Sections of Thick First-Year Sea Ice at 17 GHz, Vertical and Cross Polarizations, from the 1977, 1978, and 1979 Universtiy of Kansas Arctic Experiments.

6.0 CONCLUSIONS

The discrimination capabilities of radar as applied to the study of sea ice has been demonstrated by this and previous experiments. The objective of the University of Kansas sea ice experiment program has been to obtain quantitative measurements of radar backscatter from ice which would aid in the selection of the optimum parameters for operational ice surveillance radar systems. These parameters include the frequency, receive and transmit polarizations, and the angle of incidence.

To meet this objective, thick first-year sea ice, thin first-year sea ice, brackish sea ice, and fresh-water lake ice were investigated at 1.5 GHz and from 8-18 GHz, at angles of incidence from 10° to 75° (with respect to vertical), and with antenna transmit-receive polarizations of VV and VH for the 1.5 GHz radar and VV, HV, and HH for the 8-18 GHz radar. A transportable surface-based system, TRAMAS, and a helicopter-mounted system, HELOSCAT, were used as platforms for these radars.

The L-band (1.5 GHz) radar was found to have little ability to discriminate among the ice types studied. Some discrimination between thick and thin first-year sea ice with cross-polarization for angles of incidence greater than 40° may be possible. Results tend to confirm that the practical utilization of L-band radars would be for topographic mapping.

The Ku-X-band results indicated that the capability to discriminate among all of the ice types investigated was good provided that the proper angle of incidence was selected. With this in mind, all frequencies and all polarizations have the potential for use in a

discrimination system. The optimum combination, based on the relative levels and the degree of separation between responses for the different ice types, would be a radar operating at 9 GHz, vertical polarization, and angles of incidence greater than 40°.

A study to determine the effect of snow cover on lake ice returns was also conducted as a part of this experiment. The difference in return from snow-covered lake ice and bare-surface lake ice was very significant. Removal of the snow cover decreased the scattering coefficients by an amount averaging 8 dB or greater. This occurred for a 4 cm snow cover which indicates the importance of snow cover in the mechanisms involved in backscatter return from sea ice.

A comparison of scattering coefficient responses obtained with the TRAMAS system and the HELOSCAT system showed a high degree of similarity. This indicates that the future use of the HELOSCAT system is very promising. Differences in the absolute levels of scattering coefficient for the two systems was linked to the calibration of the HELOSCAT system. Future experiments with this system must recognize the problems associated with calibration of the HELOSCAT and take steps to correct them. Recent development of a single-antenna system for use with the HELOSCAT should greatly reduce antenna alignment problems associated with the previous system.

Comparison of the scattering coefficients for lake ice and thick first-year sea ice from the three University of Kansas sea ice experiments tends to raise more questions than it answers. This demonstrates the need for further investigation of the backscatter properties of sea ice. Experiments to pinpoint the locations and elements in the sea ice medium which contribute to the backscatter are desperately

needed. This type of information may be obtained by recording the intermediate frequency returns from the target and processing the recorded returns using Fast-Fourier-transform techniques. Apparatus which will accomplish this task has been added to the system, which will be used in the 1980 sea ice experiment. Results of this experiment will be eagerly awaited by those interested in the radar studies of sea ice.

AD-A091 239 KANSAS UNIV/CENTER FOR RESEARCH INC LAWRENCE REMOTE --ETC F/G 17/9
RADAR SCATTEROMETER MEASUREMENTS OF SEA ICE: THE SURSAT EXPERIM--ETC(U)
AUG 80 C V DELKER, R G ONSTOTT, R K MOORE N00014-76-C-1105
UNCLASSIFIED CRINC/RSL-TR 331-17 NL

END
DATE FILMED
DTIC

REFERENCES

1. Hanson, A., "Arctic Geography, Climate, and Ice," Chapter 2, Arctic Flying, Office of Naval Research, 1979.

2. Parashar, S.K., A.W. Biggs, A.K. Fung, and R.K. Moore, "Investigation of Radar Discrimination of Sea Ice," Proceedings of the Ninth International Symposium on Remote Sensing of Environment, University of Michigan, Ann Arbor, 1974.

3. Anderson, V.H., "High Altitude Side-Looking Radar Images of Sea Ice in the Arctic," Proceedings of the Fourth International Symposium on Remote Sensing of Environment, University of Michigan, Ann Arbor, 1966, pp. 845-857.

4. Rouse, J.W. (Jr.), "Arctic Ice Type Identification by Radar," Proceedings IEEE, vol. 57, 1969, pp. 605-614.

5. Johnson, J.D. and L.D. Farmer, "Use of Side-Looking Airborne Radar for Sea Ice Identification," Journal of Geophysical Research, vol. 76, no. 9, 1979, pp. 2138-2155.

6. Glushkov, V.M. and V.B. Komarov, "Side-Looking Imaging Radar System TOROS and Its Application to the Study of Ice Conditions and Geological Explorations," Proceedings of the Seventh International Symposium on Remote Sensing of Environment, University of Michigan, Ann Arbor, 1971.

7. Ketchum, R.D. and S.G. Tooma, "Analysis and Interpretation of Airborne Multi-frequency Side-Looking Radar Sea Ice Imagery," Journal of Geophysical Research, vol. 78, no. 3, 1973, pp. 520-538.

8. Dunbar, M., "Interpretation of SLAR Imagery of Sea Ice," Journal of Glaciology, vol. 15, no. 73, 1975, pp. 193-213.

9. Dunbar, M. and W.F. Weeks, "The Interpretation of Young Ice Forms in the Gulf of St. Lawrence Using Radar and IR Imagery," DREO Report No. 711, 1975, pp. 1-14.

10. Gray, L., R.O. Ramseier, and W.J. Campbell, "Scatterometer and SLAR Results Obtained over Arctic Sea Ice and Their Relevance to the Problems of Arctic Ice Reconnaissance," Fourth Canadian Symposium on Remote Sensing, P.Q., Canada, May 1977, pp. 424-443.

11. Ketchum, R.D., "An Evaluation of Side-Looking Radar Imagery of Sea Ice Features and Condition in the Lincoln Sea, Nares Strait, and Baffin Bay <U>," NORDA Technical Note 57, 1977.

12. Onstott, R.G., R.K. Moore, and W.F. Weeks, "Surface-Based Scatterometer Results of Arctic Sea Ice," IEEE Transactions on Geoscience Electronics, vol. GE-17, no. 3, July 1979, pp. 78-85.

13. Onstott, R.G., G.J. Dome, C.V. Delker, J.S. Patel, and R.K. Moore, "Radar Backscatter Study of Sea Ice," University of Kansas Center for Research, Inc., Remote Sensing Laboratory Technical Report RSL TR 331-14, Lawrence, Kansas, February 1980.

14. Patel, J.S., R.G. Onstott, C.V. Delker, and R.K. Moore, "Backscatter Measurements of Sea Ice with a Helicopter-Borne Scatterometer," University of Kansas Center for Research, Inc., Remote Sensing Laboratory Technical Report RSL TR 331-13, Lawrence, Kansas, July 1979.

15. Moore, R.K., "Microwave Remote Sensors," Chapter 9, Manual of Remote Sensing, vol. 1, American Society of Photogrammetry, 1975.

16. Moore, R.K., "Ground Echo," Chapter 25, Radar Handbook (M.I. Skolnik, editor), McGraw-Hill, 1970.

17. Waite, W.P., "Broad-Spectrum Electromagnetic Backscatter," University of Kansas Center for Research, Inc., Remote Sensing Laboratory Technical Report RSL 133-17, Lawrence, Kansas, August 1970.

18. Bush, T.F. and F.T. Ulaby, "8-18 GHz Radar Scatterometer," University of Kansas Center for Research, Inc., Remote Sensing Laboratory Technical Report RSL TR 177-43, Lawrence, Kansas, September 1973.

19. Stiles, W.H., D. Brunfeldt, and F.T. Ulaby, "Performance Analysis of the MAS (Microwave Active Spectrometer) Systems: Calibration, Precision, and Accuracy," University of Kansas Center for Research, Inc., Remote Sensing Laboratory Technical Report RSL TR 360-4, Lawrence, Kansas, April 1979.

20. Onstott, R.G., R.A. Hand, J.S. Patel, and R.K. Moore, "Transportable Microwave Active Spectrometer 'TRAMAS' or 'MAS Jr.' Design Memo," University of Kansas Center for Research, Inc., Remote Sensing Laboratory Technical Memorandum RSL TM 331-4, Lawrence, Kansas, September 1978.

21. Delker, C.V., R.G. Onstott, R.A. Hand, and R.K. Moore, "Transportable Microwave Active Spectrometer 'TRAMAS' -- Modifications Report 1," University of Kansas Center for Research, Inc., Remote Sensing Laboratory Technical Memorandum RSL TM 331-5, Lawrence, Kansas, June 1979.

22. Rossiter, J.R. and K.A. Butt, "Remote Estimation of the Properties of Sea Ice, Beaufort Sea Field Trip Report -- March 1979," C-CORE Publication Number 79-9, Centre for Cold Ocean Resources Engineering, Memorial University of Newfoundland, St. John's, Newfoundland, Canada, June 1979.

23. Delker, C.V., R.G. Onstott, and R.K. Moore, "Intermediate Results of the Radar Backscatter Study of Sea Ice in the Beaufort Sea," University of Kansas Center for Research, Inc., Remote Sensing Laboratory Technical Report RSL TR 331-15, Lawrence, Kansas, March 1980.